Mathematical modeling, simulation and order reduction of ocular flows and their interactions: Building the digital twin of the eye

Thomas Saigre[1],

supervised by Christophe Prud'homme[1] & Marcela Szopos[2]

[1]Institut de Recherche Mathématique Avancée, UMR 7501 Université de Strasbourg et CNRS

[2]Université Paris Cité, CNRS, MAP5, F-75006 Paris, France

PhD defense

20th December 2024

Context

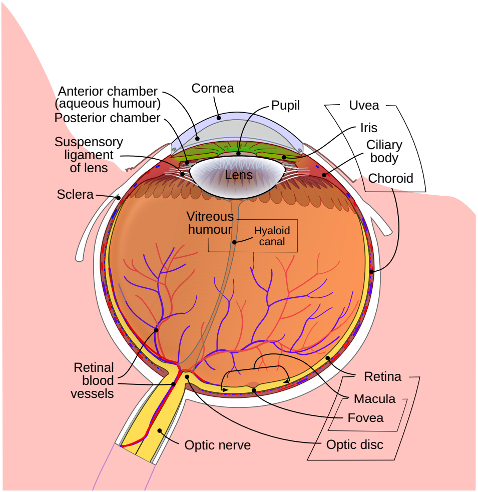

Rhcastilhos, from Wikipedia

- The **eye** is a complex organ, with a **multilayered structure**.
- Need to understand ocular **physiology** and **pathology**.
- Complexity to perform **measurements** on a human subject[a], mostly available on surface[b].
- Present work: focus on **heat transfer** and **aqueous humor flow dynamics**.

[a] Rosenbluth & Fatt. *Exp. Eye Res.* (1977)
[b] Purslow & Wolffsohn. *Eye Contact Lens.* (2005)

Context

- The **anterior chamber** (AC) is filled with **aqueous humor** (AH), whose dynamics is crucial for the ocular health[a],
- understand the **AH flow dynamics** and **heat transfer** is important for **drug distribution**[b], or ocular **therapies** (laser treatment, corneal cell sedimentation[c], etc.).

[a] Dvoriashyna *et al.* *Ocular Fluid Dynamics.* (2019)
[b] Bhandari. *J Control Release.* (2021)
[c] Kinoshita *et al.* *N Engl J Med.* (2018)

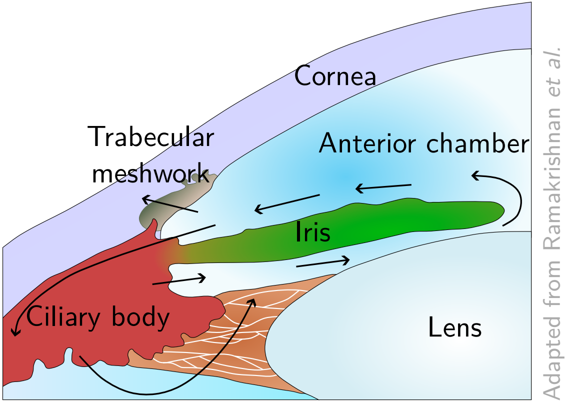

Figure 1: Production and drainage of AH in the eye.

Building the digital twin of the eye

- Based on **mathematical models**[a] of the eye.
- Data from **previous studies** and **measurements** to validate and enhance the models.

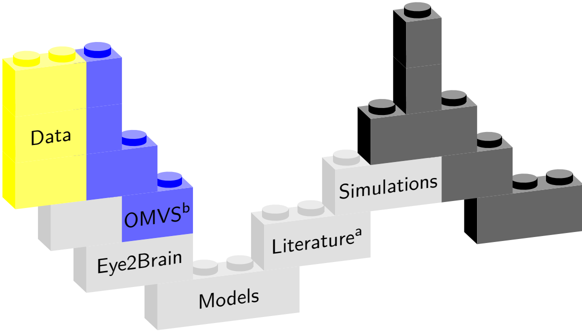

[a] Scott (1988), Ng & Ooi (2007), Dvoriashyna *et al.* (2019)...
[b] Sala *et al.* "The ocular mathematical virtual simulator" (2023).

Building the digital twin of the eye

- Based on **mathematical models**[a] of the eye.
- Data from **previous studies** and **measurements** to validate and enhance the models.

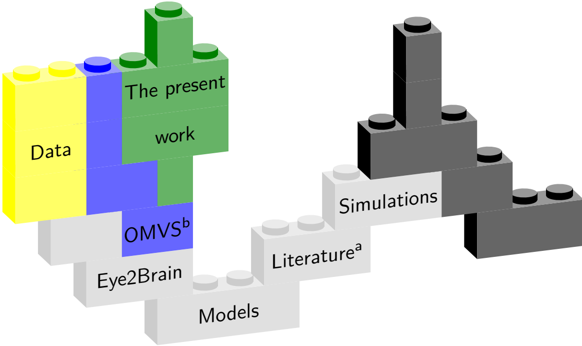

[a] Scott (1988), Ng & Ooi (2007), Dvoriashyna *et al.* (2019)...
[b] Sala *et al.* "The ocular mathematical virtual simulator" (2023).

Building the digital twin of the eye

- Based on **mathematical models**[a] of the eye.
- Data from **previous studies** and **measurements** to validate and enhance the models.
- **Digital twin:** a virtual replica of the eye.

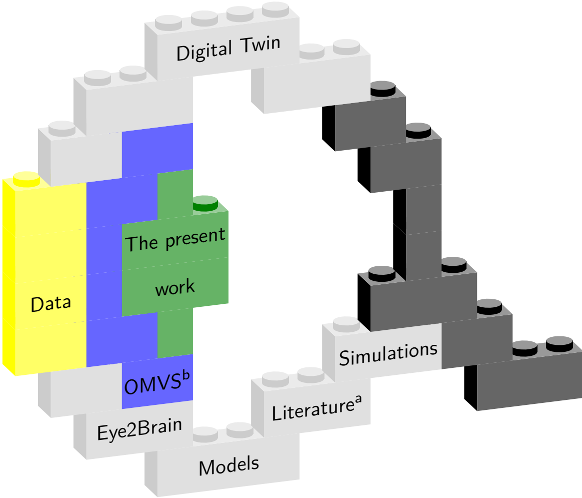

[a] Scott (1988), Ng & Ooi (2007), Dvoriashyna *et al.* (2019)...
[b] Sala *et al.* "The ocular mathematical virtual simulator" (2023).

Methodology

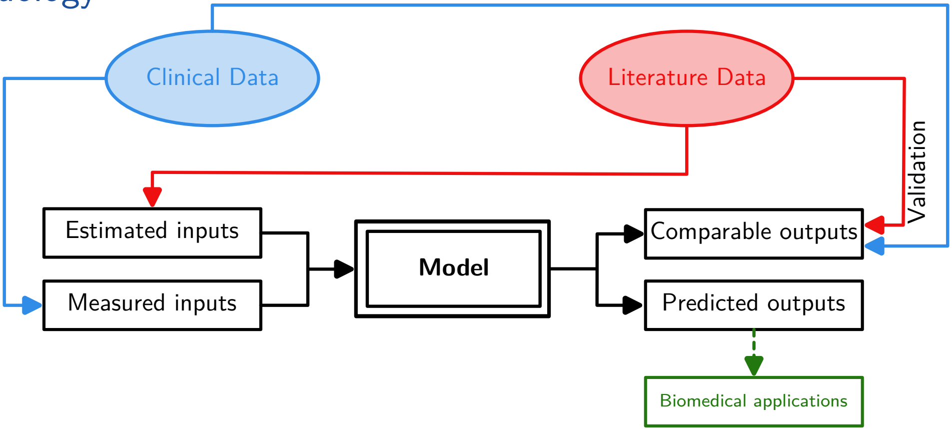

Figure 2: Methodology for the development of patient-specific models, adapted from[a].

[a] Sala *et al.* *International Journal for Numerical Methods in Biomedical Engineering*. (2023)

General framework

Model complexity

- Monophysics-Multiphysics problem
- Numerous parameters and scarce experimental data
- Influence of multiple risk factors or a combination of them

General framework

Finite element

In silico **model**

Model complexity

- Monophysics-Multiphysics problem
- Numerous parameters and scarce experimental data
- Influence of multiple risk factors or a combination of them

Sensitivity analysis

General framework

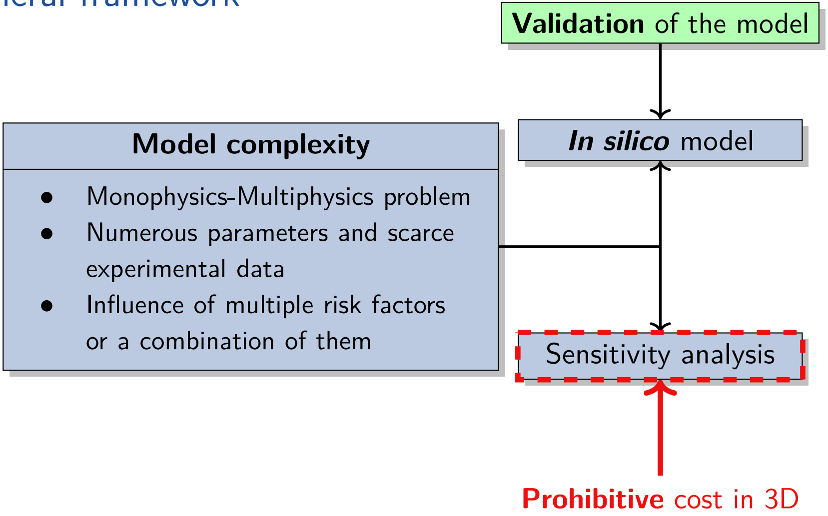

General framework

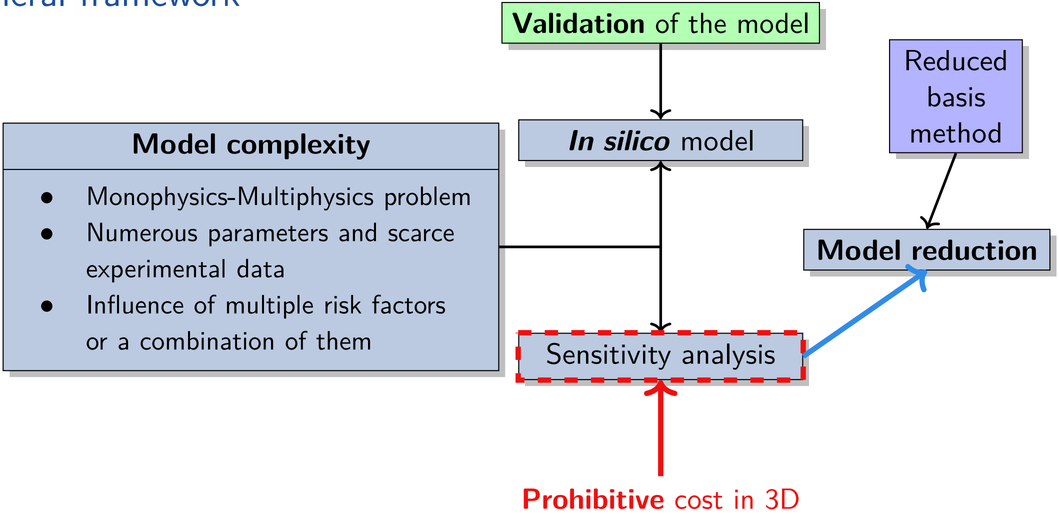

Programming and runtime environment

- **Feel++[a]:** Open source library to solve ODEs and PDEs using the **finite element** methods.
- Usage of **toolboxes** or internal **libraries** to solve complex problems.
- All the results presented here are developed and obtained within this framework.

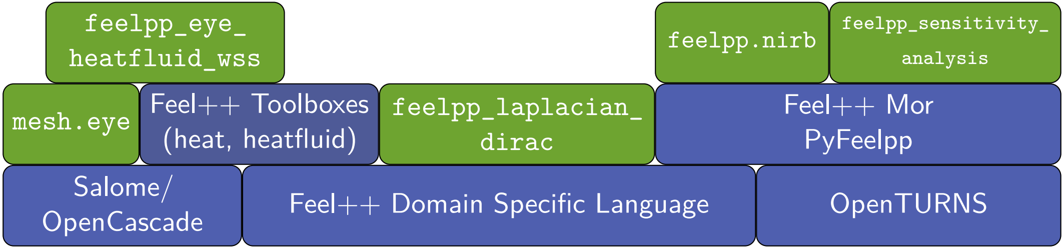

[a] C. Prud'homme, V. Chabannes V, T. Saigre *et al.* Feel++ Release V111. (2024)

`github.com/feelpp/feelpp`

Contents

Mathematical modeling of heat transfer and aqueous humor flow mechanisms in the eye

Geometrical model[a]

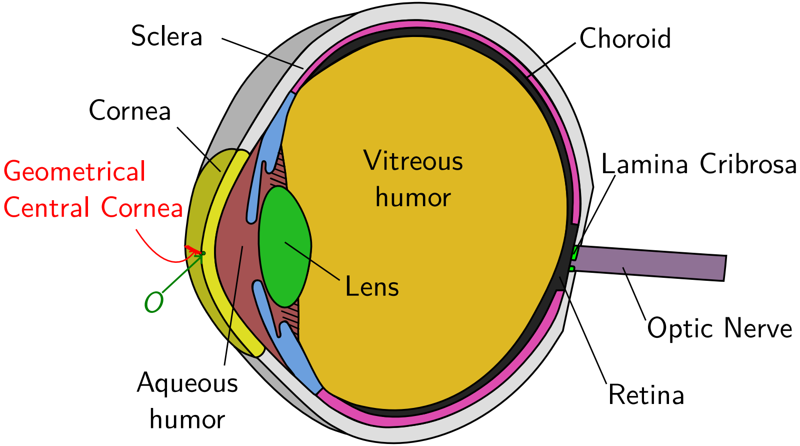

[a] Sala *et al.* The ocular mathematical virtual simulator: A validated multiscale model for hemodynamics and biomechanics in the human eye. *Int J Numer Method Biomed Eng.* (2023)

Biophysical model[a][b]

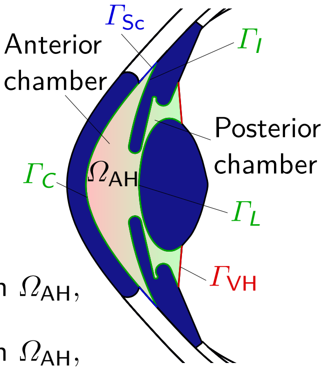

- Incompressible fluid, constant density,
- The steady flow of the aqueous humor is governed by the Navier–Stokes equations:

Navier-Stokes equations — Boussinesq approximation

$$\boxed{\rho(\boldsymbol{u}\cdot\nabla)\boldsymbol{u} - \nabla\cdot(2\mu\underline{\underline{\boldsymbol{D}}}(\boldsymbol{u}) - p\underline{\underline{\boldsymbol{I}}})} = \boxed{-\rho\beta(T - T_{\text{ref}})\boldsymbol{g}} \quad \text{in } \Omega_{\text{AH}},$$

Incompressibility

$$\nabla\cdot\boldsymbol{u} = 0 \quad \text{in } \Omega_{\text{AH}},$$

Heat transfer equation

$$\rho C_p \boldsymbol{u}\cdot\nabla T - k_i\nabla^2 T = 0 \quad \text{in } \Omega = \bigcup_i \Omega_i.$$

[a] Scott. *Physics in Medicine and Biology*. (1988), Ng & Ooi. *Comput Methods Programs Biomed*. (2006), Li *et al.* *Int J Numer Method Biomed Eng*. (2010)...

[b] Wang *et al.* *BioMedical Engineering OnLine*. (2016), Dvoriashyna *et al.* *Mathematical Models of Aqueous Production, Flow and Drainage*. (2019)...

Biophysical Model: Boundary Conditions

- Interface conditions: $\begin{cases} T_i = T_j, \\ k_i(\nabla T_i \cdot \boldsymbol{n}_i) = -k_j(\nabla T_j \cdot \boldsymbol{n}_j) \end{cases}$ over $\partial\Omega_i \cap \partial\Omega_j$.
- Robin condition on Γ_{body}: $-k_i \dfrac{\partial T}{\partial \boldsymbol{n}} = h_{\text{bl}}(T - T_{\text{bl}})$.
- Neumann condition on Γ_{amb}:
$$-k_i \frac{\partial T}{\partial \boldsymbol{n}} = h_{\text{amb}}(T - T_{\text{amb}}) + \sigma\varepsilon(T^4 - {T_{\text{amb}}}^4) + E.$$

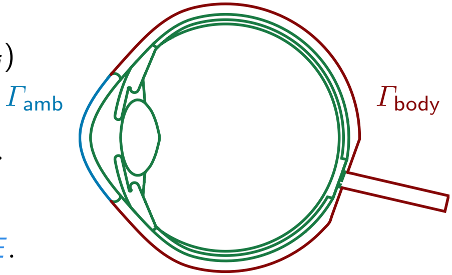

[a] Scott. *Physics in Medicine and Biology*. (1988)

Biophysical Model: Boundary Conditions

- Interface conditions: $\begin{cases} T_i = T_j, \\ k_i(\nabla T_i \cdot \boldsymbol{n}_i) = -k_j(\nabla T_j \cdot \boldsymbol{n}_j) \end{cases}$
  over $\partial\Omega_i \cap \partial\Omega_j$.
- Robin condition on Γ_{body}: $-k_i \dfrac{\partial T}{\partial \boldsymbol{n}} = h_{\text{bl}}(T - T_{\text{bl}})$.
- Linearized Neumann condition[a] on Γ_{amb}:
  $$-k_i \frac{\partial T_i}{\partial \boldsymbol{n}} = h_{\text{amb}}(T - T_{\text{amb}}) + h_{\text{r}}(T - T_{\text{amb}}) + E,$$
  with $h_{\text{r}} = 6\,\text{W}\,\text{m}^{-2}\,\text{K}^{-1}$.

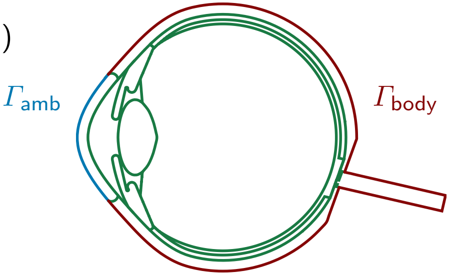

[a] Scott. *Physics in Medicine and Biology*. (1988)

Biophysical Model: Boundary Conditions

- Interface conditions: $\begin{cases} T_i = T_j, \\ k_i(\nabla T_i \cdot \boldsymbol{n}_i) = -k_j(\nabla T_j \cdot \boldsymbol{n}_j) \end{cases}$
  over $\partial\Omega_i \cap \partial\Omega_j$.
- Robin condition on Γ_{body}: $-k_i \dfrac{\partial T}{\partial \boldsymbol{n}} = h_{\text{bl}}(T - T_{\text{bl}})$.
- Linearized Neumann condition[a] on Γ_{amb}:
  $-k_i \dfrac{\partial T_i}{\partial \boldsymbol{n}} = h_{\text{amb}}(T - T_{\text{amb}}) + h_{\text{r}}(T - T_{\text{amb}}) + E$,
  with $h_{\text{r}} = 6\,\mathrm{W\,m^{-2}\,K^{-1}}$.
- Conditions on velocity:
  $\boldsymbol{u} = \boldsymbol{0}$ on $\Gamma_C \cup \Gamma_I \cup \Gamma_L \cup \Gamma_{\text{VH}} \cup \Gamma_{\text{Sc}}$.

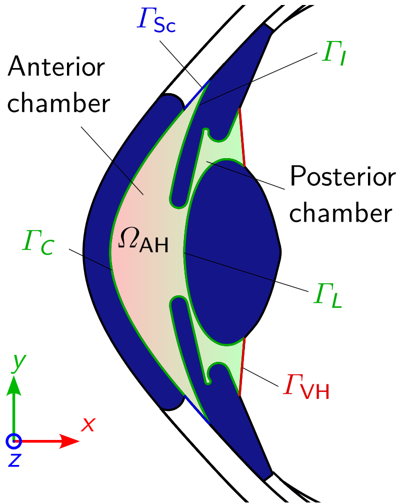

[a] Scott. *Physics in Medicine and Biology.* (1988)

Parameter dependent model

Symbol	Name	Dimension	Baseline value	Range
T_{amb}	Ambient temperature	[K]	298	[283.15, 303.15]
T_{bl}	Blood temperature	[K]	310	[308.3, 312]
h_{amb}	Ambient air convection coefficient	$[\mathrm{W\,m^{-2}\,K^{-1}}]$	10[a]	[8, 100]
h_{bl}	Blood convection coefficient	$[\mathrm{W\,m^{-2}\,K^{-1}}]$	65[b]	[50, 110]
h_{r}	Radiation heat transfer coefficient	$[\mathrm{W\,m^{-2}\,K^{-1}}]$	6[c]	–
E	Evaporation rate	$[\mathrm{W\,m^{-2}}]$	40[c]	[20, 320]
k_{lens}	Lens conductivity	$[\mathrm{W\,m^{-1}\,K^{-1}}]$	0.4[b]	[0.21, 0.544]
k_{cornea}	Cornea conductivity	$[\mathrm{W\,m^{-1}\,K^{-1}}]$	0.58[d]	–
$k_{\mathrm{sclera}} = k_{\mathrm{iris}} = k_{\mathrm{lamina}} = k_{\mathrm{opticNerve}}$	Eye envelope components conductivity	$[\mathrm{W\,m^{-1}\,K^{-1}}]$	1.0042[e]	–
$k_{\mathrm{aqueousHumor}}$	Aqueous humor conductivity	$[\mathrm{W\,m^{-1}\,K^{-1}}]$	0.28[d]	–
$k_{\mathrm{vitreousHumor}}$	Vitreous humor conductivity	$[\mathrm{W\,m^{-1}\,K^{-1}}]$	0.603[c]	–
$k_{\mathrm{choroid}} = k_{\mathrm{retina}}$	Vascular beds conductivity	$[\mathrm{W\,m^{-1}\,K^{-1}}]$	0.52[f]	–
ε	Emissivity of the cornea	[–]	0.975[a]	–

[a] Mapstone (1968), [b] J J W Lagendijk (1982), [c] Scott (1988), [d] Emery *et al.* (1975), [e] Ng & Ooi (2007), [f] IT'IS Foundation (2024).

Parameters and output of interest

- Geometrical parameters may play a role[a], but not considered in this work.
- **A parameter:** we set $\mu = (T_{\text{amb}}, T_{\text{bl}}, h_{\text{amb}}, h_{\text{bl}}, E, k_{\text{lens}})$ in $D^\mu \subset \mathbb{R}^6$.
- $\bar{\mu} \in D^\mu$ is the ***baseline value*** of the parameters.

[a] Bhandari. *J Control Release*. (2021)

- Locations of interest based on literature[b c d]:

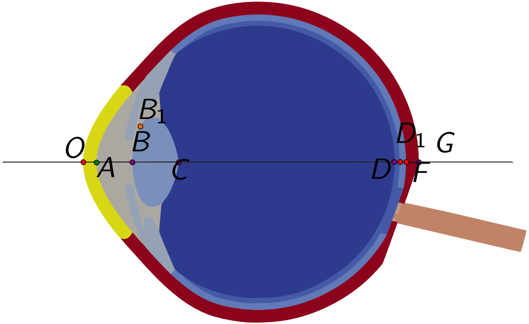

[b] Scott. *Physics in Medicine and Biology*. (1988)
[c] Ng & Ooi. *Comput. Biol. Med.* (2007)
[d] Li *et al.* *Int J Numer Method Biomed Eng*. (2010)

Summary

Parameter input μ

$$\downarrow$$

$$\boxed{\mathcal{M}}$$

$$\downarrow$$

$T(\mu), \boldsymbol{u}(\mu), p(\mu), s(\mu)$

Model $\mathcal{M}_{\mathrm{HF}}(\mu)$

- **Heat transfer** in the whole eye,
- coupled with AH **fluid dynamics** in the AC and the PC.

Model $\mathcal{M}_{\mathrm{H}}(\mu)$

- Simplified version of $\mathcal{M}_{\mathrm{HF}}(\mu)$.
- **Heat transfer** in the whole eye, with
- linearized radiative conditions.

Full order computational framework

Discrete geometry

- Performed with Salome meshing library, using NETGEN[a]meshing algorithm.
- The full pipeline to generate the mesh is available on GitHub[b].

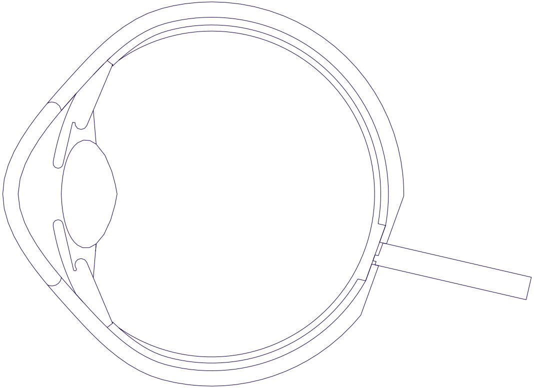

Figure 3: Geometry of the eye.

[a] J. Schöberl. *Computing and Visualization in Science.* (1997)

[b] V. Chabannes, C. Prud'homme, T. Saigre, *et al. A 3D geometrical model and meshing procedures for the human eyeball.* (2024)

Discrete geometry

- Performed with Salome meshing library, using NETGEN[a] meshing algorithm.
- The full pipeline to generate the mesh is available on GitHub[b].
- The mesh generated by Salome is quite coarse.

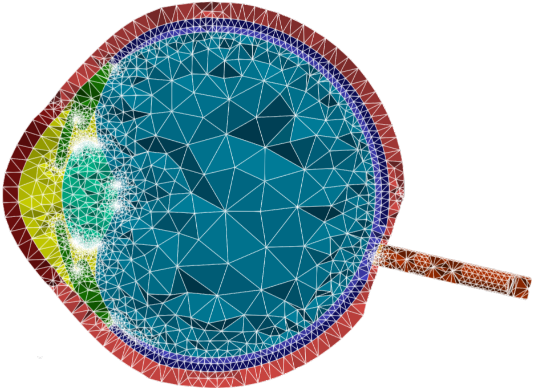

Figure 3: Original mesh $\mathtt{M}$, $4.64 \cdot 10^5$ tetrahedrons.

[a] J. Schöberl. *Computing and Visualization in Science.* (1997)

[b] V. Chabannes, C. Prud'homme, T. Saigre, *et al.* *A 3D geometrical model and meshing procedures for the human eyeball.* (2024)

Discrete geometry

- Performed with Salome meshing library, using NETGEN[a] meshing algorithm.
- The full pipeline to generate the mesh is available on GitHub[b].
- The mesh generated by Salome is quite coarse.
- We refine the mesh around the AC and PC.
- For the verification step, we generate a family of meshes of various refinement.

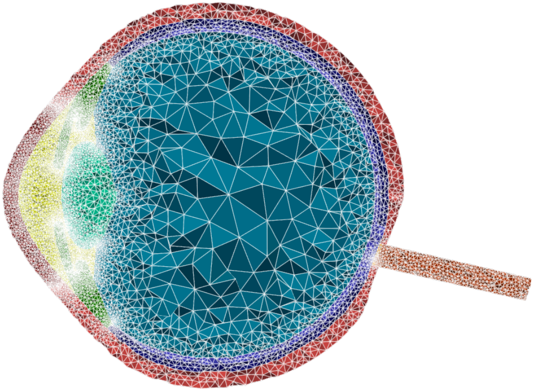

Figure 3: Mesh refined around AC and PC `Mr`, $9.4 \cdot 10^5$ elements.

[a] J. Schöberl. *Computing and Visualization in Science*. (1997)

[b] V. Chabannes, C. Prud'homme, T. Saigre, *et al.* *A 3D geometrical model and meshing procedures for the human eyeball*. (2024)

Mesh adaptation and refinement

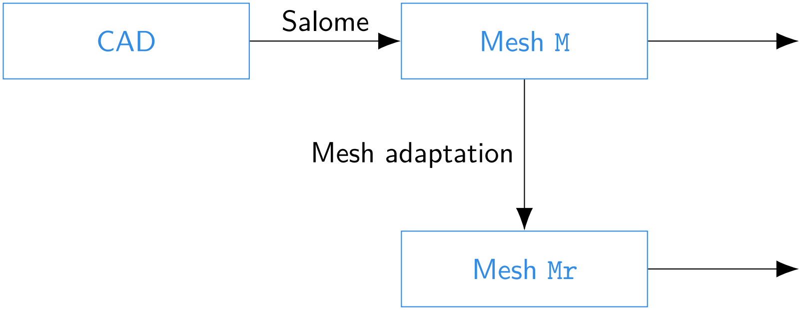

Figure 4: Pipeline to generate the geometry and mesh families.

Mesh adaptation and refinement

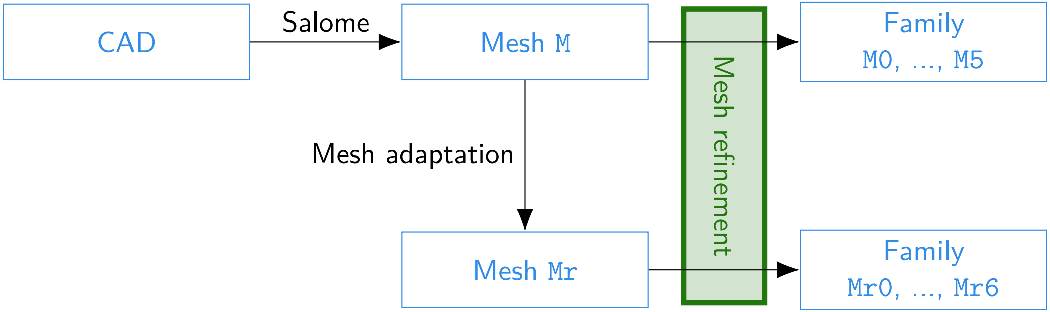

Figure 4: Pipeline to generate the geometry and mesh families.

- All the meshes are available in an open-source repository[a].

[a] T. Saigre *et al.* *Mesh and configuration files to perform coupled heat+fluid simulations on a realistic human eyeball geometry with Feel++.* (2024)

Verification steps: preservation of the volume

- Solve a Laplacian problem with manufactured solution and compare convergence with the FEM theory.
- Perform a mesh convergence study to ensure the mesh is well refined.

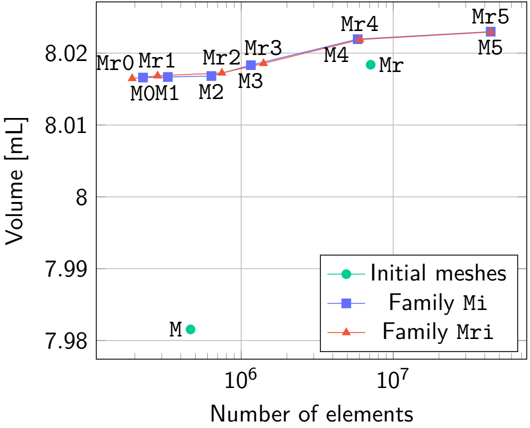

- The volume tends toward a constant value, around 8.02 mL.
- The geometric model overestimates this value, but still remains in an acceptable physiological range[a].

[a] Heymsfield *et al.* *Anatomy & Physiology*. (2016)

Continuous and discrete problem $\mathcal{M}_{\mathrm{H}}$

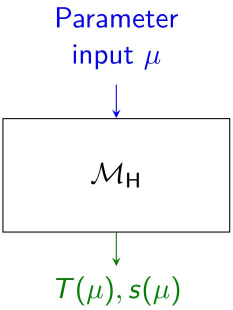

We set $V := H^1(\Omega)$.

Problem considered

Given $\mu \in D^\mu$, evaluate the output of interest

$$s(\mu) = \ell(T(\mu); \mu),$$

where $T(\mu) \in V$ is the solution of

$$a(T(\mu), v; \mu) = f(v; \mu) \quad \forall v \in V.$$

The bilinear form $a(\cdot, \cdot; \mu)$ and the linear form $f(\cdot; \mu)$ are defined by the variational formulation of the problem.

Continuous and discrete problem $\mathcal{M}_{\mathrm{H}}$

We set $V := H^1(\Omega)$

Para
inp

$T^{\mathrm{fem}}(\mu), s(\mu)$

$a(T, v; \mu) = f(v; \mu)$,

with:

$$a(T, v; \mu) := k_{\mathrm{lens}} \int_{\Omega_{\mathrm{lens}}} \nabla T \cdot \nabla v \,\mathrm{d}x + \sum_{i \neq \mathrm{lens}} k_i \int_{\Omega_i} \nabla T \cdot \nabla v \,\mathrm{d}x +$$

$$\int_{\Gamma_{\mathrm{amb}}} \left[h_{\mathrm{amb}} T + h_r T\right] v \,\mathrm{d}\sigma + \int_{\Gamma_{\mathrm{body}}} h_{\mathrm{bl}} T v \,\mathrm{d}\sigma$$

$$f(v; \mu) := \int_{\Gamma_{\mathrm{amb}}} \left[h_{\mathrm{amb}} T_{\mathrm{amb}} + h_r T_{\mathrm{amb}} - E\right] v \,\mathrm{d}\sigma + \int_{\Gamma_{\mathrm{body}}} h_{\mathrm{bl}} T_{\mathrm{bl}} v \,\mathrm{d}\sigma.$$

The bilinear form $a(\cdot, \cdot; \mu)$ and the linear form $f(\cdot; \mu)$ are defined by the variational formulation of the problem.

Continuous and discrete problem $\mathcal{M}_{\mathrm{H}}$

Parameter input μ

$$\downarrow$$

$$\boxed{\mathcal{M}_{\mathrm{H}}^{\mathrm{fem}}}$$

$$\downarrow$$

$T^{\mathrm{fem}}(\mu), s(\mu)$

We set $V := H^1(\Omega)$. Denote by $V_h \subset V$ a finite-dimensional subspace of V of dimension $\mathcal{N}$.

High-fidelity model

Given $\mu \in D^\mu$, evaluate the output of interest

$$s(\mu) = \ell(T^{\mathrm{fem}}(\mu); \mu),$$

where $T^{\mathrm{fem}}(\mu) \in V_h$ is the solution of

$$a(T^{\mathrm{fem}}(\mu), v; \mu) = f(v; \mu) \quad \forall v \in V_h.$$

The bilinear form $a(\cdot, \cdot; \mu)$ and the linear form $f(\cdot; \mu)$ are defined by the variational formulation of the problem.

Continuous and discrete problem $\mathcal{M}_{\mathrm{H}}$

Parameter input μ

$\downarrow$

$\boxed{\mathcal{M}_{\mathrm{H}}^{\mathrm{fem}}}$

$\downarrow$

$T^{\mathrm{fem}}(\mu), s(\mu)$

High fidelity resolution

Input: $\mu \in D^{\mu}$,

- Construct $\underline{\underline{\boldsymbol{A}}}(\mu)$, $\boldsymbol{f}(\mu)$ and $\boldsymbol{L}_k(\mu)$,
- Solve $\underline{\underline{\boldsymbol{A}}}(\mu)\boldsymbol{T}^{\mathrm{fem}}(\mu) = \boldsymbol{f}(\mu)$,
- Compute outputs $s(\mu) = \boldsymbol{L}_k(\mu)^T \boldsymbol{T}^{\mathrm{fem}}(\mu)$.

Output: Numerical solution $\boldsymbol{T}^{\mathrm{fem}}(\mu)$ and outputs $s(\mu)$.

High Fidelity model $\mathcal{M}_{\mathrm{H}}^{\mathrm{fem}}$

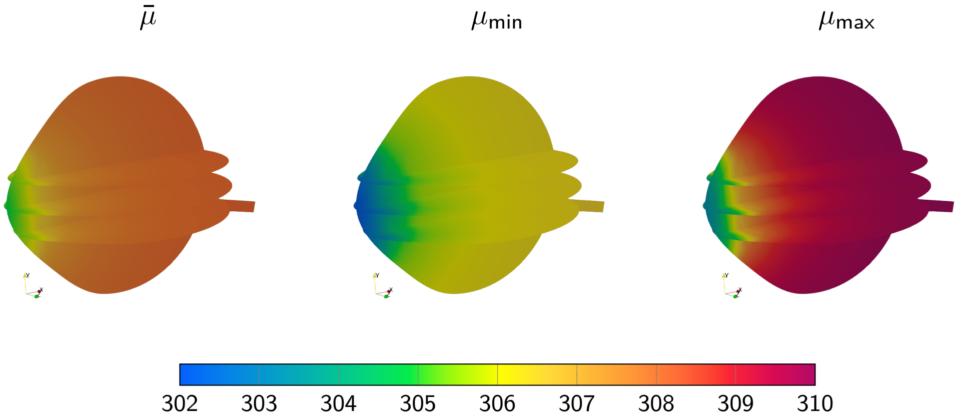

Figure 5: Distribution of the temperature [K] in the eyeball from the linear model.

Comparison with previous **numerical** studies

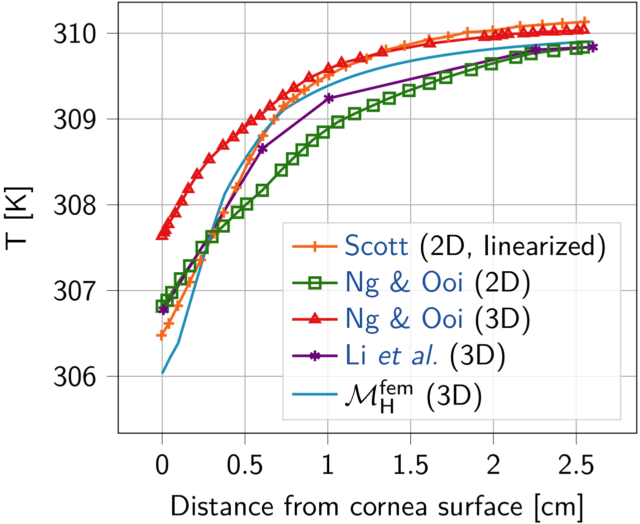

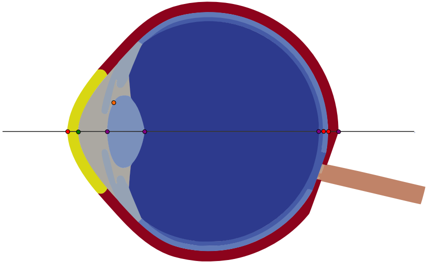

Validation: **measured** values over the GCC

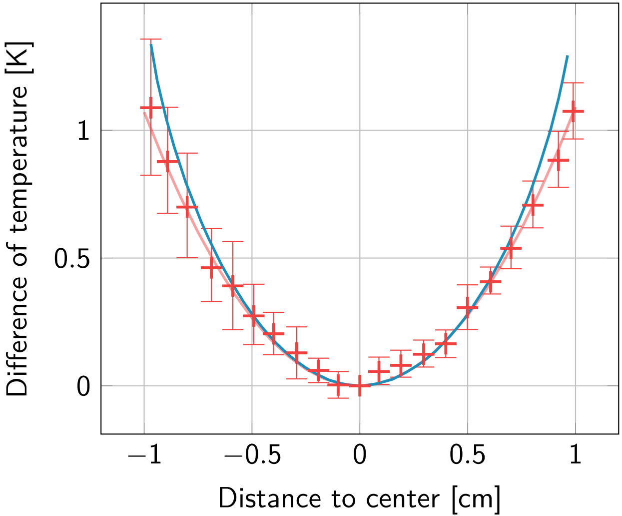

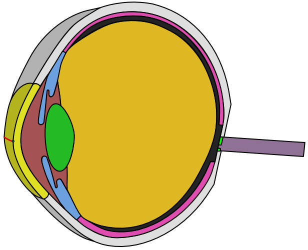

[a] Efron *et al.* *Current Eye Research.* (1989)

Reduced order computational framework

Model Order Reduction

- **Goal:** replicate input-output behavior of the high fidelity model $\mathcal{M}_{\mathrm{H}}^{\mathrm{fem}}$ with a reduced order model $\mathcal{M}_{\mathrm{H}}^{\mathrm{rbm}}$,
- with a procedure stable and efficient.

Parameter input μ

$\downarrow$

$\mathcal{M}_{\mathrm{H}}^{\mathrm{fem}}(\mu)$
(high fidelity)

$\downarrow$

$T^{\mathrm{fem}}(\mu), s(\mu)$

Model Order Reduction

- **Goal:** replicate input-output behavior of the high fidelity model $\mathcal{M}_{\mathrm{H}}^{\mathrm{fem}}$ with a reduced order model $\mathcal{M}_{\mathrm{H}}^{\mathrm{rbm}}$,
- with a procedure stable and efficient.

Parameter input μ

$\mathcal{M}_{\mathrm{H}}^{\mathrm{fem}}(\mu)$
(high fidelity)

$T^{\mathrm{fem}}(\mu), s(\mu)$

Parameter input μ

$\mathcal{M}_{\mathrm{H}}^{\mathrm{rbm}}(\mu)$

$T^{\mathrm{rbm},N}(\mu), s_N(\mu)$

$\mathcal{N} \gg N$

Model Order Reduction

Mathematical and numerical methods for model order reduction:

- Proper orthogonal decomposition[a]
- Reduced Basis method[b]
- Non-Intrusive Reduced Basis[c]
- Machine learning techniques, such as Physics-Informed Neural Networks[d]

---

[a] Kerschen *et al.* *Nonlinear Dynamics*. (2005)
[b] Prud'homme *et al.* *Journal of Fluids Engineering*. (2002)
[c] Chakir & Maday. *Comptes Rendus Mathématique*. (2009)
[d] Raissi *et al.* *Journal of Computational Physics*. (2019)

Model Order Reduction

Mathematical and numerical methods for model order reduction:

- Proper orthogonal decomposition[a]
- Reduced Basis method[b]
- Non-Intrusive Reduced Basis[c]
- Machine learning techniques, such as Physics-Informed Neural Networks[d]

[a] Kerschen *et al.* *Nonlinear Dynamics*. (2005)
[b] Prud'homme *et al.* *Journal of Fluids Engineering*. (2002)
[c] Chakir & Maday. *Comptes Rendus Mathématique*. (2009)
[d] Raissi *et al.* *Journal of Computational Physics*. (2019)

Reduced basis method[a]

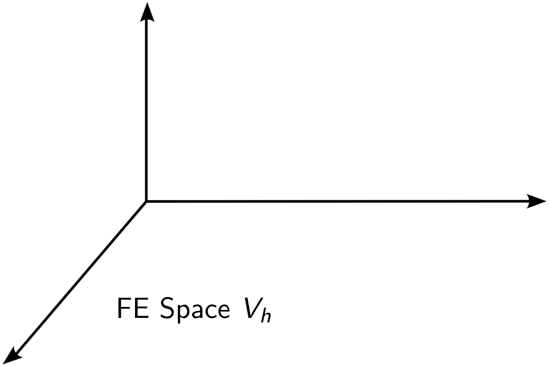

[a] Prud'homme *et al.* *Journal of Fluids Engineering*. (2002)

Reduced basis method[a]

- High fidelity model:
  $\mathcal{M}_{\mathrm{H}}^{\mathrm{fem}} : \mu \mapsto T^{\mathrm{fem}}(\mu)$

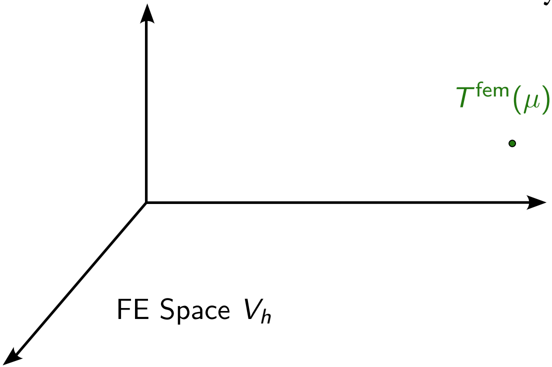

[a] Prud'homme *et al.* *Journal of Fluids Engineering*. (2002)

Reduced basis method[a]

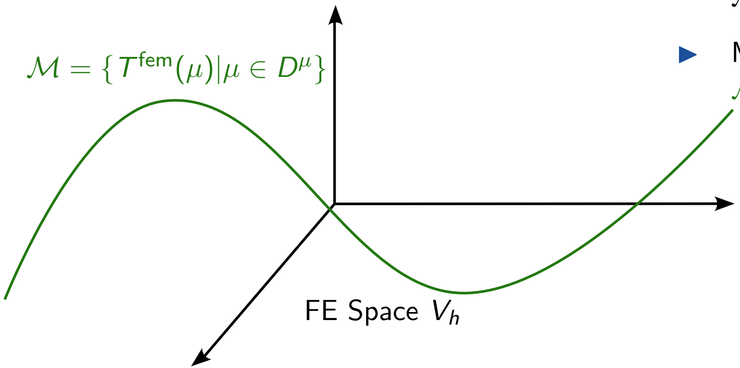

- High fidelity model:
  $\mathcal{M}_{\mathrm{H}}^{\text{fem}}: \mu \mapsto T^{\text{fem}}(\mu)$
- Manifold of solutions:
  $\mathcal{M} = \{T^{\text{fem}}(\mu), \mu \in D^\mu\}$

[a] Prud'homme *et al.* *Journal of Fluids Engineering*. (2002)

Reduced basis method[a]

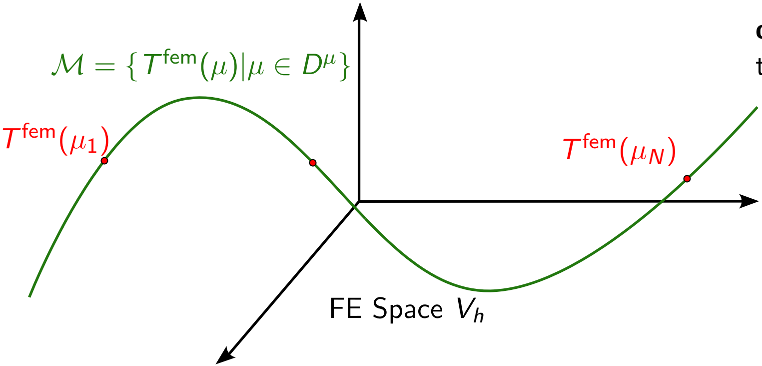

- From a set of **snapshots** $T^{\text{fem}}(\mu_1), \cdots, T^{\text{fem}}(\mu_N)$ computed **only once** (*offline stage*), we define the **reduced functional space**:

[a] Prud'homme *et al.* *Journal of Fluids Engineering*. (2002)

Reduced basis method[a]

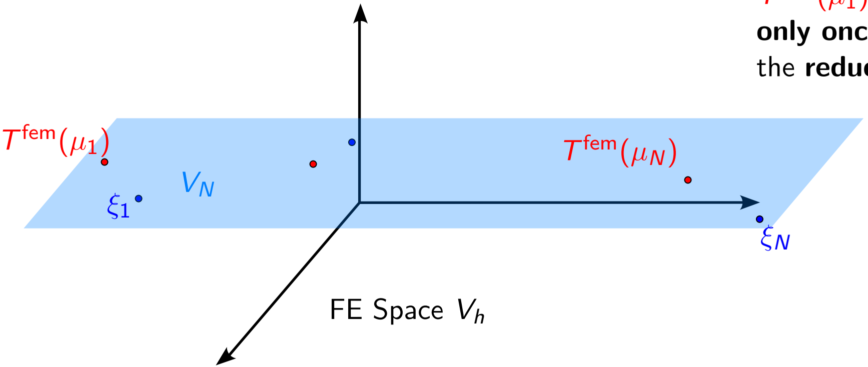

- From a set of **snapshots** $T^{\text{fem}}(\mu_1), \cdots, T^{\text{fem}}(\mu_N)$ computed **only once** (*offline stage*), we define the **reduced functional space**:

$$V_N = \text{span}(\xi_1, \cdots, \xi_N)$$

where $\xi_i = T^{\text{fem}}(\mu_i)$, is orthonormalized.

[a] Prud'homme *et al.* *Journal of Fluids Engineering*. (2002)

Reduced basis method[a]

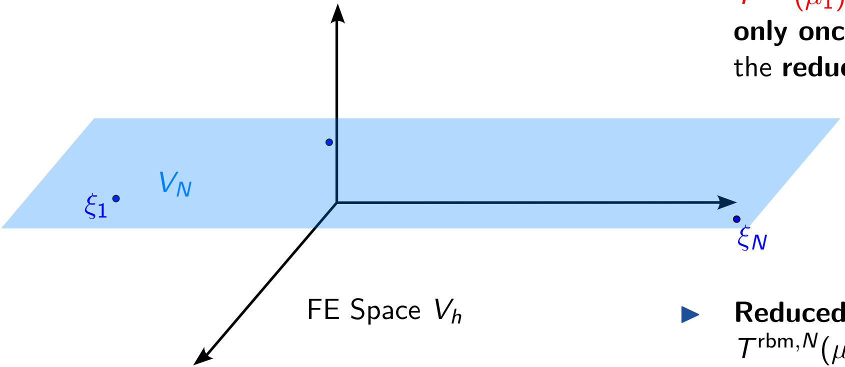

- From a set of **snapshots** $T^{\text{fem}}(\mu_1), \cdots, T^{\text{fem}}(\mu_N)$ computed **only once** (*offline stage*), we define the **reduced functional space**:

$$V_N = \text{span}(\xi_1, \cdots, \xi_N)$$

where $\xi_i = T^{\text{fem}}(\mu_i)$, is orthonormalized.

- **Reduced solution (*online stage*):** $T^{\text{rbm},N}(\mu)$ solution of the PDE on V_N, **independant** of $\mathcal{N}$.

[a] Prud'homme *et al.* *Journal of Fluids Engineering*. (2002)

Certified error bound $\Delta_N(\mu)$[a]

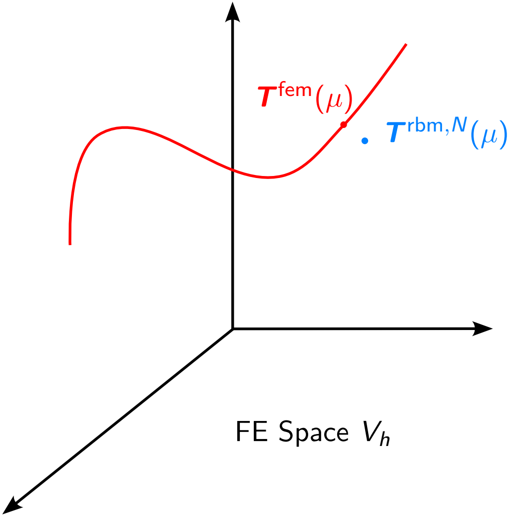

For $\mu \in D^\mu$, we define the error:

$$e(\mu) = \boldsymbol{T}^{\text{fem}}(\mu) - \boldsymbol{T}^{\text{rbm},N}(\mu).$$

[a] Prud'homme *et al.* *Journal of Fluids Engineering*. (2002)

Certified error bound $\Delta_N(\mu)$[a]

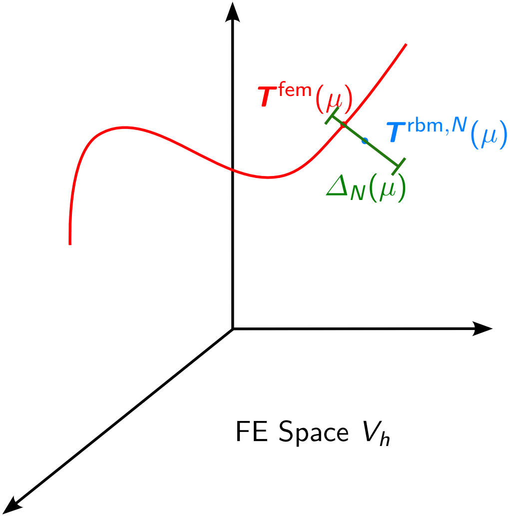

For $\mu \in D^\mu$, we define the error:

$$e(\mu) = \boldsymbol{T}^{\text{fem}}(\mu) - \boldsymbol{T}^{\text{rbm},N}(\mu).$$

We require this error bound to be:

- **Rigorous**: $\|e(\mu)\|_X \leqslant \Delta_N(\mu)$,
- **sharp**: $\dfrac{\Delta_N(\mu)}{\|e(\mu)\|_X} \leqslant \eta_{\max}(\mu)$,
- **efficient**: the computation of $\Delta_N(\mu)$ does not depend on $\mathcal{N}$.

[a] Prud'homme *et al.* *Journal of Fluids Engineering*. (2002)

Time of execution

Implementation in the Feel++ library.

	Finite element resolution $T^{\text{fem}}(\mu)$			Reduced model $T^{\text{rbm},N}(\mu), \Delta_N(\mu)$
	$\mathbb{P}_1$	$\mathbb{P}_2$ (np=1)	$\mathbb{P}_2$ (np=12)	
Problem size	$\mathcal{N} = 207\,845$	$\mathcal{N} = 1\,580\,932$		$N = 10$
t_{exec}	5.534 s	62.432 s	10.76 s	2.88×10^{-4} s
speed-up	11.69	1	5.80	$\mathbf{2.17 \times 10^5}$

Table 1: Times of execution, using mesh `M3` for high fidelity simulations.

Results over a sampling $\Xi_{\text{test}} \subset D^{\mu}$ of 100 parameters

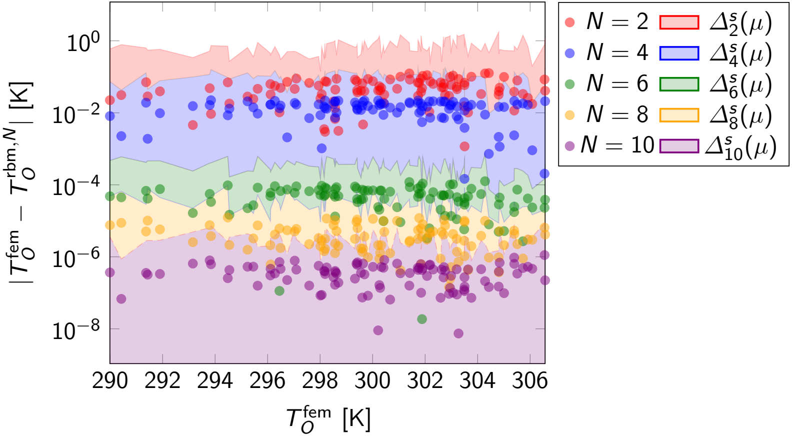

Figure 6: Error on RBM for various reduced basis sizes with error bound $\Delta_N(\mu)$.

Results over a sampling $\Xi_{\text{test}} \subset D^\mu$ of 100 parameters

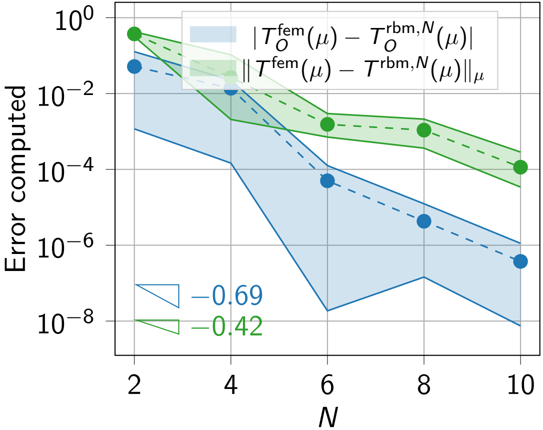

Figure 6: Convergence of the errors on the field and the output on point O.

Pointwise output

- We relied on the fact that the output functional $\ell\colon T \mapsto s(T(\mu);\mu)$ is continuous with respect to the solution T.
- ⚠ In the models considered, the output is the temperature at a specific point, *e.g.* $\ell(T(\mu)) = \delta_O(T(\mu))$, which is **non-continuous** with respect to T.

[a] Köppl & Wohlmuth. *SIAM Journal on Numerical Analysis*. (2014)
[b] Bertoluzza *et al.* *Numerical Methods for Partial Differential Equations*. (2018)

Pointwise output

- We relied on the fact that the output functional $\ell\colon T \mapsto s(T(\mu);\mu)$ is continuous with respect to the solution T.
- In the models considered, the output is the temperature at a specific point, *e.g.* $\ell(T(\mu)) = \delta_O(T(\mu))$, which is **non-continuous** with respect to T.
- Some theoretical and numerical studies[a] [b] were carried on problem of the form

$$\begin{cases} -\Delta u = \delta_{\mathbf{x}_0} & \text{in } \Omega, \\ +\text{various boundary conditions} & \text{on } \partial\Omega. \end{cases}$$

- Impact of the position of the Dirac with respect to the boundary of the domain.
- Our numerical findings show that the theoretical results are pessimistic.

[a] Köppl & Wohlmuth. *SIAM Journal on Numerical Analysis*. (2014)
[b] Bertoluzza *et al.* *Numerical Methods for Partial Differential Equations*. (2018)

Conclusions on Model Order Reduction

- Used the **Certified Reduced Basis Method** to reduce the computational cost of the high fidelity model $\mathcal{M}_{\mathrm{H}}$.
- Implementation returned satisfactory results of speed-up and accuracy.

Conclusions on Model Order Reduction

- Used the **Certified Reduced Basis Method** to reduce the computational cost of the high fidelity model $\mathcal{M}_{\mathrm{H}}$.
- Implementation returned satisfactory results of speed-up and accuracy.

Other contributions in the field of model order reduction:

- Implementation of the **Non-Intrusive Reduced Basis Method**[a].
- Application to the heat transfer model of the human eye.

[a] Chakir & Maday. *Comptes Rendus Mathématique*. (2009)

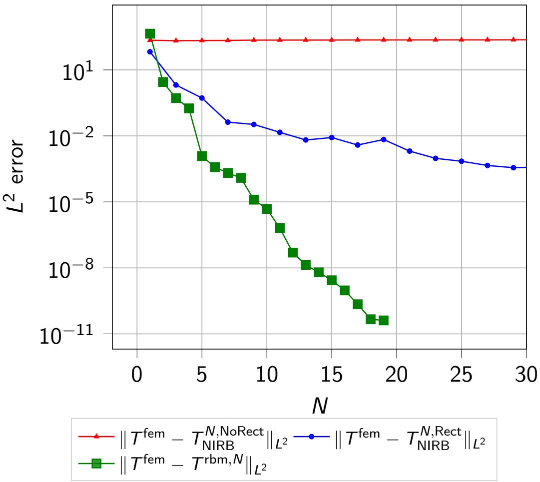

Figure 7: Comparison between RBM and NIRB accuracy, applied to model $\mathcal{M}_{\mathrm{H}}$.

Sensitivity analysis

Sensitivity analysis

- **Quantifies** the effect of input parameters on the output.
- Two studies were carried:
  1. **Deterministic** sensitivity analysis: all parameters are set to their baseline values, except for one, which varies within the ranges found in the literature,
  2. **Stochastic** sensitivity analysis: all parameters are considered as random variables.

Sobol' indices[a]

- $\mu = (\mu_1, \dots, \mu_n) \in D^\mu$,
- $\mu_i \sim X_i$ where $(X_i)_i$ is a family of **independent** random variables.
- Distributions X_i selected from data available in the literature.
- Output $s_N(\mu) \sim Y = f(X_1, \dots, X_n)$.

Sobol' indices

- **First-order indices:** $S_j = \dfrac{\mathrm{Var}\left(\mathbb{E}\left[Y|X_j\right]\right)}{\mathrm{Var}(Y)}$ effect of one parameter on the output
- **Total-order indices:** $S_j^{\mathrm{tot}} = \dfrac{\mathrm{Var}\left(\mathbb{E}\left[Y|X_{(-j)}\right]\right)}{\mathrm{Var}(Y)}$ interaction of all parameters but one on the output

where $X_{(-j)} = (X_1, \dots, X_{j-1}, X_{j+1}, \dots, X_n)$.

[a] Sobol. *Sensitivity Estimates for Nonlinear Mathematical Models.* (1993)

Input parameters distributions

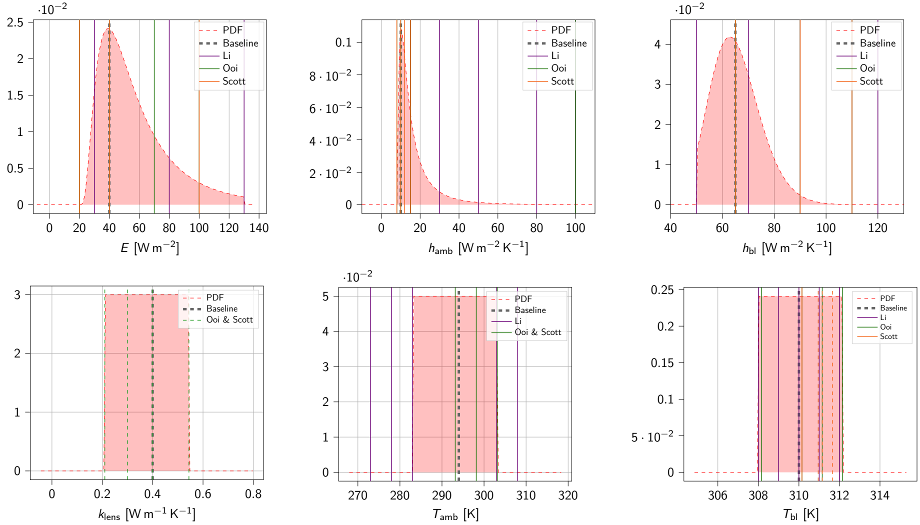

Stochastic sensitivity analysis

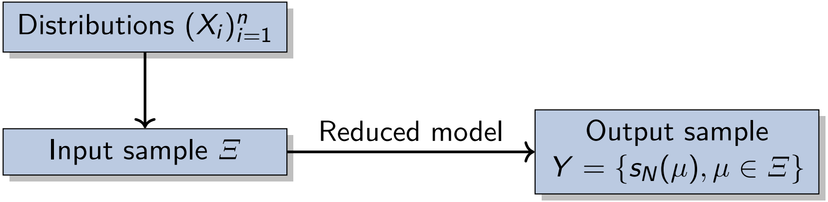

[a] Baudin *et al.* *Handbook of Uncertainty Quantification.* (2016)

Stochastic sensitivity analysis

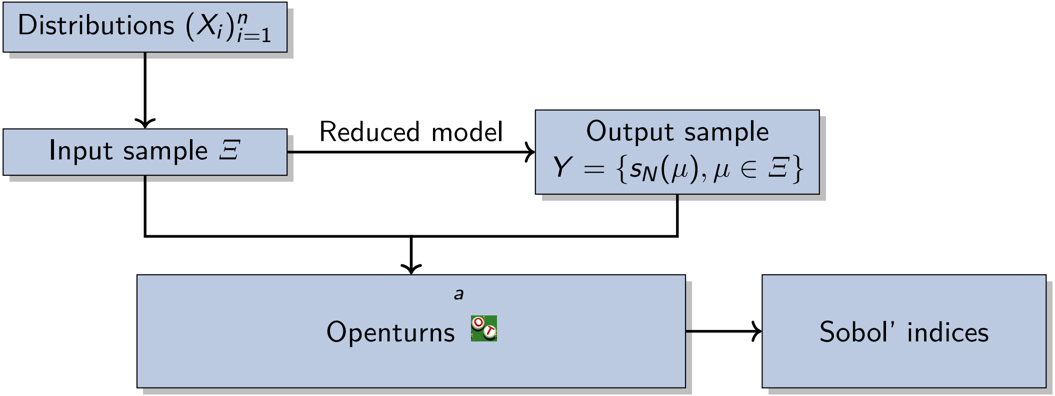

[a] Baudin *et al.* *Handbook of Uncertainty Quantification.* (2016)

Stochastic sensitivity analysis

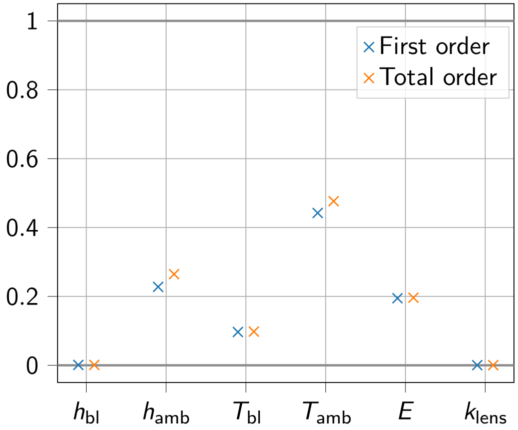

Figure 8: Sobol' indices: temperature at point O.

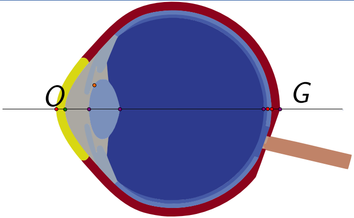

Temperature at the level of the **cornea**:

- **significantly** influenced by T_{amb}, h_{amb} (external factors) and E, T_{bl} (subject specific parameters) $\longrightarrow$ need for measurements/better model for these contributions,
- **minimally** influenced by k_{lens}, h_{bl} $\longrightarrow$ can be fixed at baseline value,
- **high order** interactions on T_{amb}, h_{amb}.

Stochastic sensitivity analysis

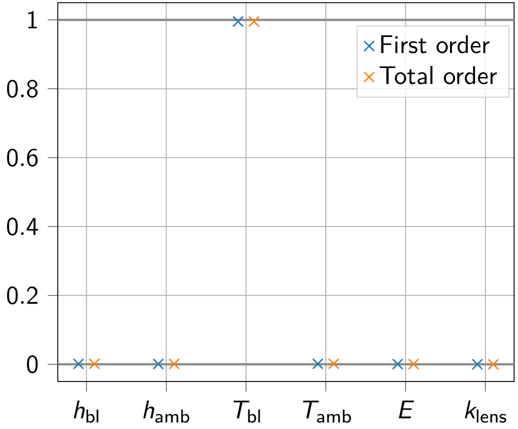

Figure 8: Sobol' indices: temperature at point G.

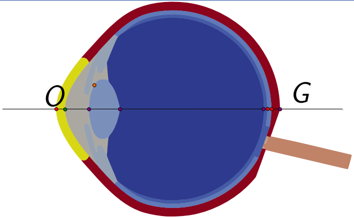

Temperature at the back of the eye:

- only influenced by the blood temperature.

Heat transfer coupled with aqueous humor flow

Motivation: Endothelial cells sedimentation

- AH flow plays a significant role in heat distribution, and intraocular pressure[a].
- Focus on the **wall shear stress** of the AH.
- Medical application: **corneal endothelial cell sedimentation** in the cornea[b].

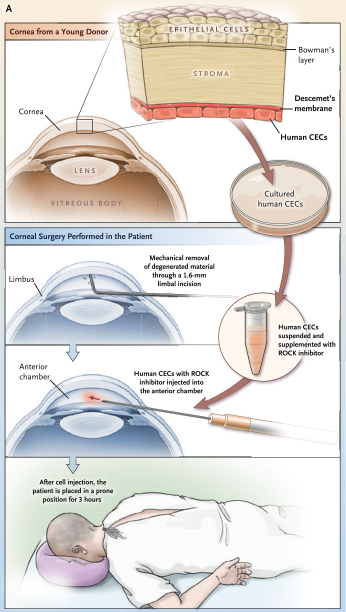

[a] Dvoriashyna *et al.* *Ocular Fluid Dynamics.* (2019)

[b] Kinoshite *et al.* *N Engl J Med.* (2018) (Figure extracted from this reference)

Computational framework of $\mathcal{M}_{\mathrm{HF}}$

Geometrical model

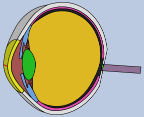

Mesh generation

- 3D mesh with **$4.97 \cdot 10^6$ elements**,
- **Fine mesh refinement** in Ω_{AH}, where the coupled model is considered.

Biophysical model $\mathcal{M}_{\mathrm{HF}}$

$$
\begin{aligned}
\rho(\boldsymbol{u} \cdot \nabla)\boldsymbol{u} - \nabla(2\mu \underline{\underline{\boldsymbol{D}}}(\boldsymbol{u}) - p\underline{\boldsymbol{I}}) &= -\rho\beta(T - T_{\mathrm{ref}})\boldsymbol{g} && \text{in } \Omega_{\mathrm{AH}},\\
\nabla \cdot \boldsymbol{u} &= 0 && \text{in } \Omega_{\mathrm{AH}},\\
\rho C_p \boldsymbol{u} \cdot \nabla T - k\nabla^2 T &= 0 && \text{in } \Omega.
\end{aligned}
$$

Finite element solver

- Use the Feel++ **heatfluid** toolbox using monolithic approach and **PDE based preconditioning** for solving the **non-linear** problem,
- ✔ Model validation and verification.

Pressure and velocity: impact of the posture

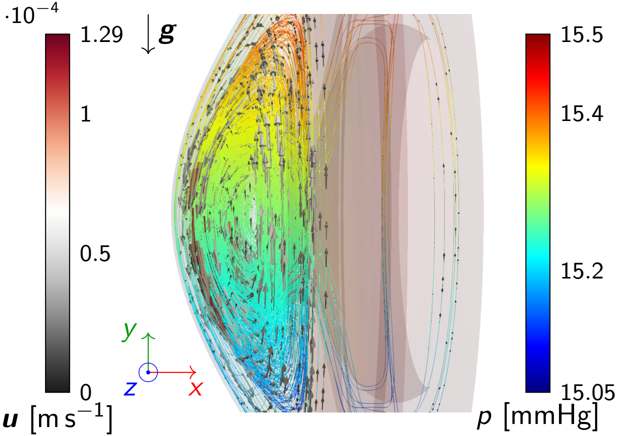

Figure 9: Standing position.

- **Recirculation** of the AH,

[a] Wang *et al.* BioMedical Engineering OnLine. (2016)
[b] Abdelhafid *et al.* *Recent Devel. in Mathematical, Statistical and Computational Sciences.* (2021)
[c] Murgoitio-Esandi *et al.* *Translational Vision Science & Technology.* (2023)

Pressure and velocity: impact of the posture

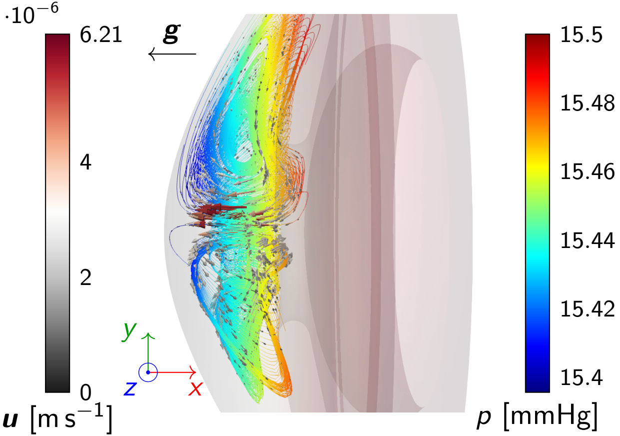

Figure 9: Prone position.

- **Recirculation** of the AH,
- Formation of a **Krukenberg's spindle**, in good agreement with clinical observations and previous studies[a][b][c]

[a] Wang *et al.* BioMedical Engineering OnLine. (2016)
[b] Abdelhafid *et al.* *Recent Devel. in Mathematical, Statistical and Computational Sciences.* (2021)
[c] Murgoitio-Esandi *et al.* *Translational Vision Science & Technology.* (2023)

Pressure and velocity: impact of the posture

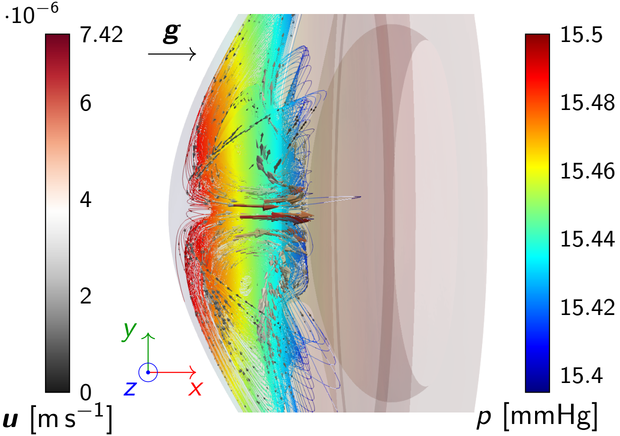

Figure 9: Supine position.

- **Recirculation** of the AH,
- Formation of a **Krukenberg's spindle**, in good agreement with clinical observations and previous studies[a][b][c]
- Fluid dynamics is **strongly influenced by the position of the patient**.

[a] Wang *et al.* BioMedical Engineering OnLine. (2016)
[b] Abdelhafid *et al.* *Recent Devel. in Mathematical, Statistical and Computational Sciences.* (2021)
[c] Murgoitio-Esandi *et al.* *Translational Vision Science & Technology.* (2023)

Wall shear stress

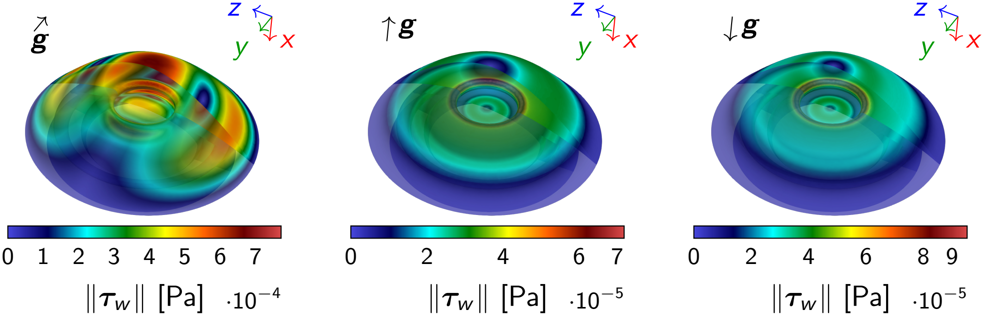

(a) Standing. (b) Prone. (c) Supine.

Figure 10: Wall shear stress distribution on the corneal endothelium for the three postural orientations.

Wall shear stress

- The WSS distribution is **impacted** by the postural orientation and the ambient temperature.
- **Application:** Control the temperature to enhance the diffusion and the sedimentation of the cells during the treatment.

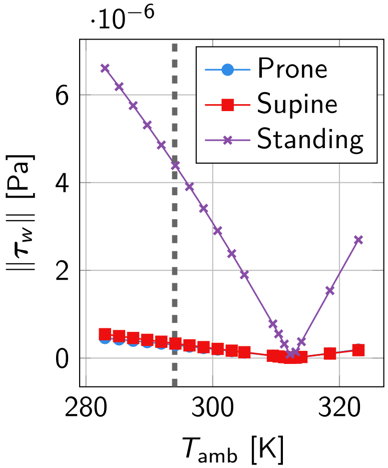

Figure 10: Mean wall shear stress on the corneal surface.

Conclusion and perspectives

- **Heat transport model in the human eye:** FEM simulations, validation against experimental data,
- **Reduced model** with a **certified error bound**,
- **Sensitivity analysis:** computation of Sobol' indices, highlight of the impact of some parameters on the outputs of interest.

- T. Saigre, C. Prud'homme, M. Szopos. Model order reduction and sensitivity analysis for complex heat transfer simulations inside the human eyeball. *Int J Numer Methods Biomed Eng*. (2024)
- T. Saigre, C. Prud'homme, M. Szopos. Associated dataset (publicly available).

  DOI: `10.5281/ZENODO.13907890` *Zenodo*. (2024)

Conclusion and perspectives

- **Couple heat transfer with AH dynamics:** assess the impact of postural orientation and environmental conditions on the flow and its properties.
  - T. Saigre, V. Chabannes, C. Prud'homme, M. Szopos. A coupled fluid-dynamics-heat transfer model for 3D simulations of the aqueous humor flow in the human eye. *CMBE2024 Proceedings*. (2024)
  - T. Saigre, C. Prud'homme, M. Szopos, V. Chabannes. Mesh and configuration files to perform coupled heat+fluid simulations on a realistic human eyeball geometry with Feel++, DOI: `10.5281/ZENODO.13886143` *Zenodo*. (2024)

- Mathematical modeling of **microbiota** and **PINNs**: CEMRACS 2023 project.
  - P. Hossie, B. Laroche, T. Malou, L. Perrin, T. Saigre, L. Sala. Surrogate modeling of interactions in microbial communities through Physics-Informed Neural Networks. *ESAIM: Proceegings and Surveys*. (2024)

Conclusion and perspectives

- **Enhance the model:**
  - **Geometrical model:** take into account geometrical parameters,
  - **Fluid dynamics:** modeling the production and drainage of aqueous humor to assess their impact.
- **Clinical perspective:** assess the corneal cell sedimentation after injection.

T. Saigre, V. Chabannes, G. Guidoboni, C. Prud'homme, M. Szopos, SP. Srinivas. Effect of Cooling of the Ocular Surface on Endothelial Cell Sedimentation in Cell Injection Therapy: Insights from Computational Fluid Dynamics. (2024), submitted to ARVO 2025 meeting.

Conclusion and perspectives

- **Enhance the model:**
  - **Geometrical model:** take into account geometrical parameters,
  - **Fluid dynamics:** modeling the production and drainage of aqueous humor to assess their impact.
- **Clinical perspective:** assess the corneal cell sedimentation after injection.

T. Saigre, V. Chabannes, G. Guidoboni, C. Prud'homme, M. Szopos, SP. Srinivas. Effect of Cooling of the Ocular Surface on Endothelial Cell Sedimentation in Cell Injection Therapy: Insights from Computational Fluid Dynamics. (2024), submitted to ARVO 2025 meeting.

- Steps towards a **digital twin** of the eye:
  - incorporate patient-specific data,
  - enhance predictive modeling and personalized medical applications.

Conclusion and perspectives

- **Enhance the model:**
  - **Geometrical model:** take into account geometrical parameters,
  - **Fluid dynamics:** modeling the production and drainage of aqueous humor to assess their impact.
- **Clinical perspective:** assess the corneal cell sedimentation after injection.
- T. Saigre, V. Chabannes, G. Guidoboni, C. Prud'homme, M. Szopos, SP. Srinivas. Effect of Cooling of the Ocular Surface on Endothelial Cell Sedimentation in Cell Injection Therapy: Insights from Computational Fluid Dynamics. (2024), submitted to ARVO 2025 meeting.
- Steps towards a **digital twin** of the eye:
  - incorporate patient-specific data,
  - enhance predictive modeling and personalized medical applications.

Thank you for your attention!

Bibliography

1. Rosenbluth, R. F. *et al.* Temperature measurements in the eye. *Experimental Eye Research* **25,** 325–341 (Oct. 1977).
2. Purslow, C. *et al.* Ocular Surface Temperature: A Review. *Eye & Contact Lens: Science & Clinical Practice* **31,** 117–123 (May 2005).
3. Dvoriashyna, M. *et al.* in *Ocular Fluid Dynamics* (eds Guidoboni, G. *et al.*) Series Title: Modeling and Simulation in Science, Engineering and Technology, 227–263 (Springer International Publishing, Cham, 2019).
4. Bhandari, A. Ocular Fluid Mechanics and Drug Delivery: A Review of Mathematical and Computational Models. *Pharmaceutical Research* **38,** 2003–2033 (Dec. 2021).
5. Li, E. *et al.* Modeling and simulation of bioheat transfer in the human eye using the 3D alpha finite element method (αFEM). *International Journal for Numerical Methods in Biomedical Engineering* **26,** 955–976 (2010).
6. Kinoshita, S. *et al.* Injection of Cultured Cells with a ROCK Inhibitor for Bullous Keratopathy. *New England Journal of Medicine* **378,** 995–1003 (Mar. 2018).
7. Ramakrishnan, R *et al.* in *Diagnosis and Management of Glaucoma* 76–76 (Jaypee Brothers Medical Publishers (P) Ltd., 2013).

Bibliography

8. Scott, J. A. A finite element model of heat transport in the human eye. *Physics in Medicine and Biology* **33,** 227–242 (Feb. 1988).

9. Ng, E. *et al.* Ocular surface temperature: A 3D FEM prediction using bioheat equation. *Computers in Biology and Medicine* **37,** 829–835 (June 2007).

10. Sala, L. *et al.* The ocular mathematical virtual simulator: A validated multiscale model for hemodynamics and biomechanics in the human eye. *International Journal for Numerical Methods in Biomedical Engineering,* e3791 (Nov. 2023).

11. Prud'homme, C. *et al.* *feelpp/feelpp: Feel++ Release V111 preview.10.* July 2024.

12. Ng, E. *et al.* FEM simulation of the eye structure with bioheat analysis. *Computer Methods and Programs in Biomedicine* **82,** 268–276 (June 2006).

13. Wang, W. *et al.* Fluid and structure coupling analysis of the interaction between aqueous humor and iris. *BioMedical Engineering OnLine* **15,** 133 (Dec. 2016).

14. Mapstone, R. Measurement of corneal temperature. *Experimental Eye Research* **7,** 237–IN29 (Apr. 1968).

15. J J W Lagendijk. A mathematical model to calculate temperature distributions in human and rabbit eyes during hyperthermic treatment. *Physics in Medicine & Biology* **27,** 1301–1311 (Nov. 1982).

Bibliography

16. Emery, A. F. *et al.* Microwave Induced Temperature Rises in Rabbit Eyes in Cataract Research. *Journal of Heat Transfer* **97,** 123–128 (Feb. 1975).

17. IT'IS Foundation. *Thermal Conductivity.* 2024.

18. Schöberl, J. NETGEN An advancing front 2D/3D-mesh generator based on abstract rules. *Computing and Visualization in Science* **1,** 41–52 (July 1997).

19. Chabannes, V. *et al.* *A 3D geometrical model and meshing procedures for the human eyeball.* Sept. 2024.

20. Saigre, T. *et al.* *Mesh and configuration files to perform coupled heat+fluid simulations on a realistic human eyeball geometry with Feel++.* Oct. 2024.

21. Heymsfield, S. B. *et al.* Adult Human Ocular Volume: Scaling to Body Size and Composition. *Anatomy & Physiology* **6** (2016).

22. Efron, N. *et al.* Ocular surface temperature. *Current Eye Research* **8,** 901–906 (Sept. 1989).

23. Kerschen, G. *et al.* The Method of Proper Orthogonal Decomposition for Dynamical Characterization and Order Reduction of Mechanical Systems: An Overview. *Nonlinear Dynamics* **41,** 147–169 (Aug. 2005).

24. Prud'homme, C. *et al.* Reliable Real-Time Solution of Parametrized Partial Differential Equations: Reduced-Basis Output Bound Methods. *Journal of Fluids Engineering* **124,** 70–80 (Mar. 2002).

Bibliography

25. Chakir, R. *et al.* Une méthode combinée d'éléments finis à deux grilles/bases réduites pour l'approximation des solutions d'une E.D.P. paramétrique. *Comptes Rendus. Mathématique* **347.** Publisher: Elsevier, 435–440 (2009).

26. Raissi, M. *et al.* Physics-informed neural networks: A deep learning framework for solving forward and inverse problems involving nonlinear partial differential equations. *Journal of Computational Physics* **378,** 686–707 (2019).

27. Christophe Prud'homme *et al.* *feelpp/feelpp: Feel++ Release V111 preview.9.* Mar. 2024.

28. Köppl, T. *et al.* Optimal A Priori Error Estimates for an Elliptic Problem with Dirac Right-Hand Side. *SIAM Journal on Numerical Analysis* **52,** 1753–1769 (Jan. 2014).

29. Bertoluzza, S. *et al.* Local error estimates of the finite element method for an elliptic problem with a Dirac source term. *Numerical Methods for Partial Differential Equations* **34,** 97–120 (Jan. 2018).

30. Sobol, I. M. *Sensitivity Estimates for Nonlinear Mathematical Models.* in (1993).

31. Baudin, M. *et al.* in *Handbook of Uncertainty Quantification* (eds Ghanem, R. *et al.*) 1–38 (Springer International Publishing, Cham, 2016).

Bibliography

32. Abdelhafid, F. *et al.* in *Recent Developments in Mathematical, Statistical and Computational Sciences* (eds Kilgour, D. M. *et al.*) Series Title: Springer Proceedings in Mathematics & Statistics, 489–499 (Springer International Publishing, Cham, 2021).

33. Murgoitio-Esandi, J. *et al.* A Mechanistic Model of Aqueous Humor Flow to Study Effects of Angle Closure on Intraocular Pressure. *Translational Vision Science & Technology* **12,** 16 (Jan. 2023).

34. Saigre, T. *et al.* Model order reduction and sensitivity analysis for complex heat transfer simulations inside the human eyeball. *International Journal for Numerical Methods in Biomedical Engineering* **40,** e3864 (Sept. 2024).

35. Saigre, T. *et al.* *Model order reduction and sensitivity analysis for complex heat transfer simulations inside the human eyeball.* Oct. 2024.

36. Saigre, T. *et al.* *A coupled fluid-dynamics-heat transfer model for 3D simulations of the aqueous humor flow in the human eye.* in *8th International Conference on Computational and Mathematical Biomedical Engineering – CMBE2024 Proceedings* **2** (P. Nithiarasu and R. Löhner (Eds.), Arlington (Virginia), United States, June 2024), 508–512.

37. Hossie, P. J. *et al.* *Surrogate modeling of interactions in microbial communities through Physics-Informed Neural Networks.*. Feb. 2024.

Bibliography

38. Saigre, T. *et al.* *Effect of Cooling of the Ocular Surface on Endothelial Cell Sedimentation in Cell Injection Therapy: Insights from Computational Fluid Dynamics.* 2024.

39. Ooi, E.-H. *et al.* Simulation of aqueous humor hydrodynamics in human eye heat transfer. *Computers in Biology and Medicine* **38,** 252–262 (Feb. 2008).

40. Karampatzakis, A. *et al.* Numerical model of heat transfer in the human eye with consideration of fluid dynamics of the aqueous humour. *Physics in Medicine and Biology* **55,** 5653–5665 (Oct. 2010).

41. Bhandari, A. *et al.* Effect of aging on heat transfer, fluid flow and drug transport in anterior human eye: A computational study. *Journal of Controlled Release* **328,** 286–303 (Dec. 2020).

42. Cybenko, G. Approximation by superpositions of a sigmoidal function. *Mathematics of Control, Signals, and Systems* **2,** 303–314 (Dec. 1989).

Linearization of the radiative transfer equation[a]

$$-k\frac{\partial T}{\partial \boldsymbol{n}} = \underbrace{h_{\text{amb}}(T - T_{\text{amb}})}_{(i)} + \underbrace{\sigma\varepsilon(T^4 - T_{\text{amb}}^4)}_{(ii)} + \underbrace{E}_{(iii)} \quad \text{on } \Gamma_{\text{amb}}.$$

(i) Convective heat transfer.

(ii) Radiative heat transfer.

(iii) Tear evaporation.

[a] Scott *Physics in Medicine and Biology*. (1988)

Linearization of the radiative transfer equation[a]

$$-k\frac{\partial T}{\partial \boldsymbol{n}} = \underbrace{h_{\mathrm{amb}}(T - T_{\mathrm{amb}})}_{(i)} + \underbrace{\sigma\varepsilon(T^4 - T_{\mathrm{amb}}^4)}_{(ii)} + \underbrace{E}_{(iii)} \quad \text{on } \varGamma_{\mathrm{amb}}.$$

(i) Convective heat transfer.

(ii) Radiative heat transfer.

(iii) Tear evaporation.

$$-k\frac{\partial T_i}{\partial \boldsymbol{n}} = h_{\mathrm{amb}}(T - T_{\mathrm{amb}}) + h_{\mathrm{r}}(T - T_{\mathrm{amb}}) + E \qquad \text{on } \varGamma_{\mathrm{amb}},$$

with $h_{\mathrm{r}} = 6\,\mathrm{W\,m^{-2}\,K^{-1}}$.

[a] Scott *Physics in Medicine and Biology*. (1988)

Linearization of the radiative transfer equation

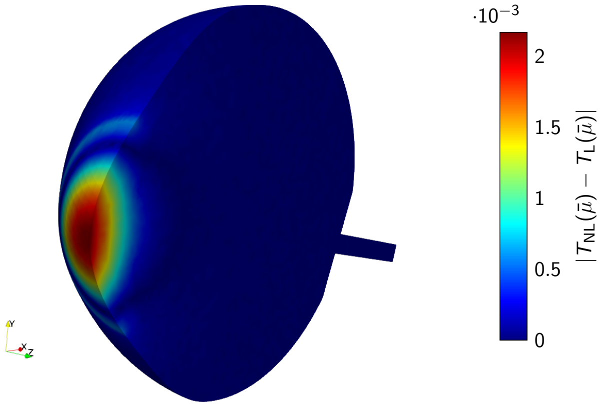

Figure 11: Difference of the temperature between the full model and the linearized model.

Mesh convergence for the high-fidelity model

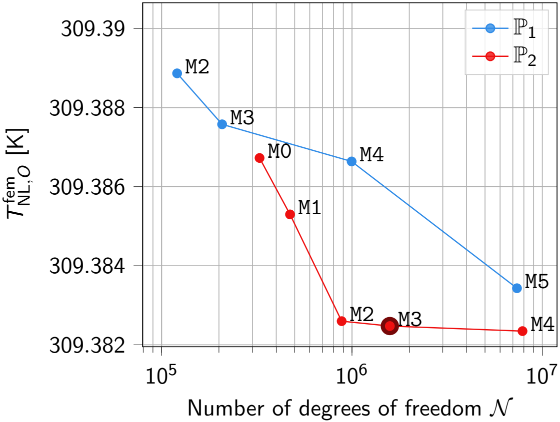

Figure 12: Temperature at the center of the cornea computed with the high-fidelity model $\mathcal{E}_{\text{NL}}(\bar{\mu})$, depending on the level of mesh refinement.

Deterministic sensitivity analysis

- We choose one parameter among the 6 parameters of the model,
- We fix the other ones to their baseline value,
- We make the selected parameter vary to study the impact of this single parameter on the output of the model.

Deterministic sensitivity analysis

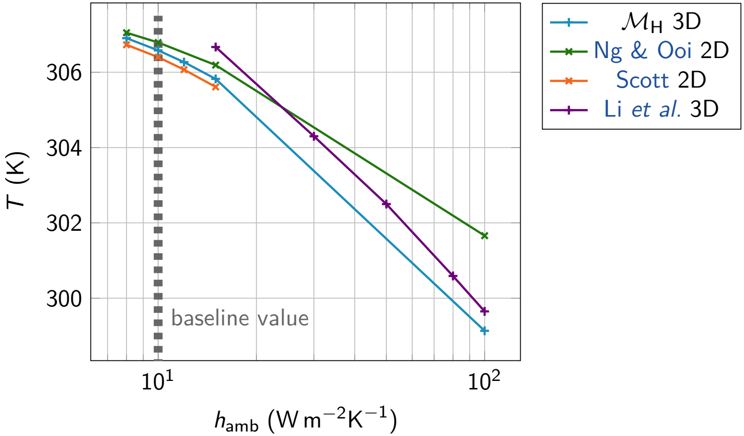

Figure 13: Effect of h_{amb} at point O

Deterministic sensitivity analysis

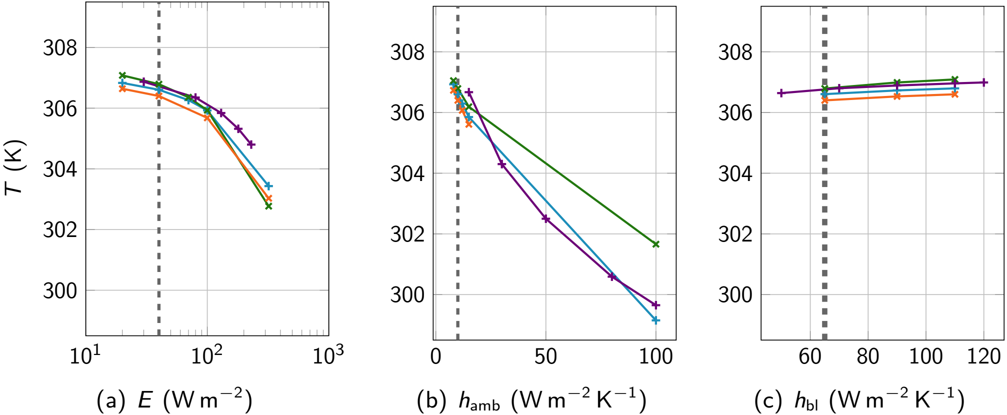

Figure 13: Point O (Current model, Ng & Ooi, Scott, Li *et al.*)

Deterministic sensitivity analysis

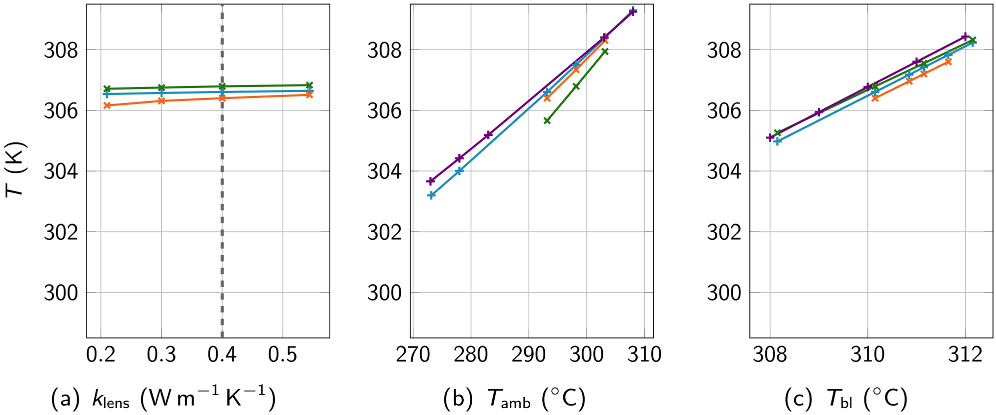

Figure 13: Point O (Current model, Ng & Ooi, Scott, Li *et al.*)

Laplacian problem with Dirac source

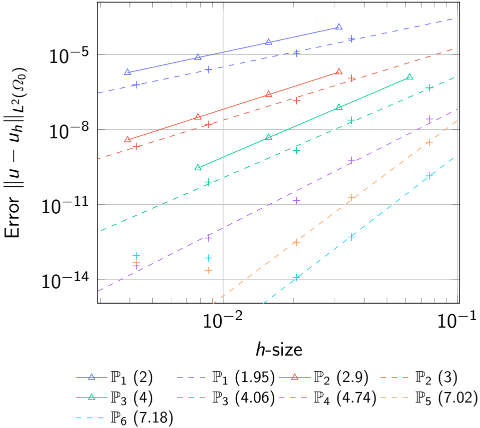

(a) Error L^2.

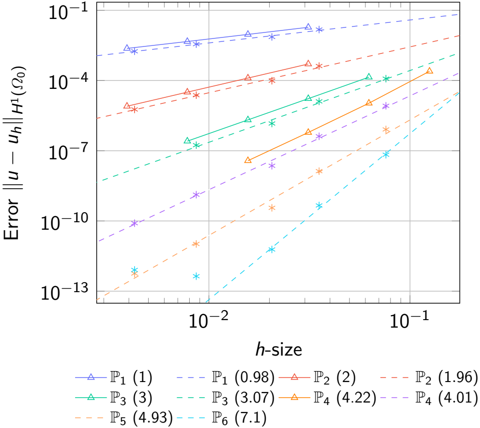

(b) Error H^1.

Laplacian problem with Dirac source

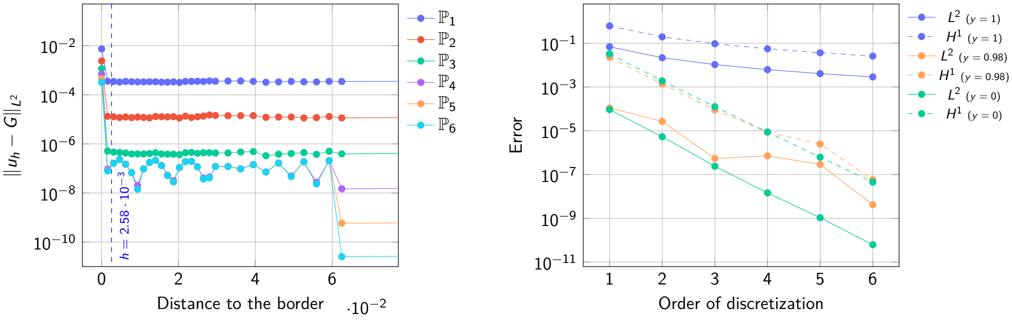

(c) Evolution of the error L^2. The vertical line shows the size of the mesh around the point $\boldsymbol{X}_0$.

(d) Evolution of the error against the order of discretization, for various y positions of the Dirac source.

Verifications and validations of the coupled heat-fluid model: mesh convergence

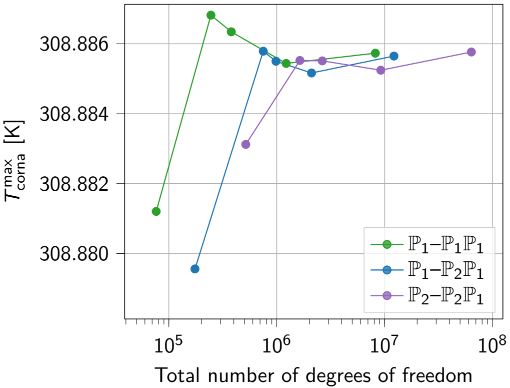

(e) Maximal temperature of the cornea.

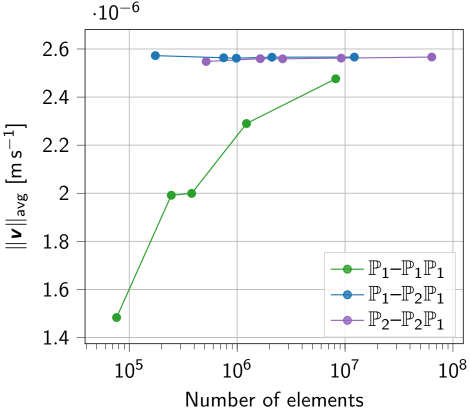

(f) Mean fluid velocity.

Verifications and validations of the coupled heat-fluid model

Author	T_{amb}	No AH flow	AH flow coupled		
			Prone	Supine	Standing
Scott (2D)	293.15	306.4	–	–	–
Ooi & Ng (2D)	298	306.45	–	–	306.9
Karampatzakis & Samaras (3D)	293	306.81	–	–	307.06
	296	307.33	–	–	307.51
	298	307.69	–	–	307.83
Current model (3D)	293	306.5647	306.56915	306.55899	306.63672
	296	307.09845	307.10175	307.09436	307.14651
	298	307.45746	307.46008	307.45432	307.49222

Verifications and validations of the coupled heat-fluid model

Position	Reference	Maximum velocity [$\mathrm{m\,s^{-1}}$]	Average velocity [$\mathrm{m\,s^{-1}}$]	Pressure [mmHg]
Supine	Wang *et al.*	$9.44 \cdot 10^{-4}$	$4.1 \cdot 10^{-5}$	$13.50 - 13.58$
	Murgoitio-Esandi *et al.*	$6 \cdot 10^{-5}$	n/a	n/a
	Bhandari *et al.*	n/a	$9.88 \cdot 10^{-6}$	n/a
	Current model	$2.59 \cdot 10^{-5}$	$3.21 \cdot 10^{-6}$	$15.42 - 15.59$
Standing	Wang *et al.*	$9.6 \cdot 10^{-4}$	$2.5 \cdot 10^{-4}$	$13.50 - 13.59$
	Bhandari *et al.*	n/a	$5.88 \cdot 10^{-5}$	n/a
	Current model	$2.76 \cdot 10^{-4}$	$5.23 \cdot 10^{-5}$	$15.28 - 15.72$

Preconditioning of the non-linear coupled heat-fluid model

$$\left[\begin{array}{cc|c} \underline{\underline{\widetilde{A}}} & \underline{\underline{B}}^T & \underline{\underline{D}} \\ \underline{\underline{B}} & \underline{\underline{0}} & \underline{\underline{0}} \\ \hline \underline{\underline{E}} & \underline{\underline{0}} & \underline{\underline{\widetilde{F}}} \end{array}\right] \left[\begin{array}{c} \underline{\Delta u} \\ \underline{\Delta p} \\ \hline \underline{\Delta T} \end{array}\right] = \left[\begin{array}{c} \underline{r}_u \\ \underline{r}_p \\ \hline \underline{r}_T \end{array}\right] \iff: \underbrace{\left[\begin{array}{c|c} \underline{\underline{K}}_{0,0} & \underline{\underline{K}}_{0,1} \\ \hline \underline{\underline{K}}_{1,0} & \underline{\underline{K}}_{1,1} \end{array}\right]}_{=:\underline{\underline{K}}} \begin{bmatrix} \underline{\Delta}_{\text{fluid}} \\ \underline{\Delta}_{\text{heat}} \end{bmatrix} = \begin{bmatrix} \underline{r}_{\text{fluid}} \\ \underline{r}_{\text{heat}} \end{bmatrix}.$$

The main idea of *additive fieldsplit* preconditioner is to approximate the inverse of the matrix $\underline{\underline{K}}$ by the matrix

$$\begin{bmatrix} \underline{\underline{K}}_{0,0}^{-1} & \underline{\underline{0}} \\ \underline{\underline{0}} & \underline{\underline{K}}_{1,1}^{-1} \end{bmatrix},$$

where the inverses of the diagonal blocks are applied separately, with appropriate solvers and associated preconditioners.

Preconditioning of the non-linear coupled heat-fluid model

The main idea of *additive fieldsplit* preconditioner is to approximate the inverse of the matrix $\underline{\underline{\boldsymbol{K}}}$ by the matrix

$$\begin{bmatrix} \underline{\underline{\boldsymbol{K}}}_{0,0}^{-1} & \underline{\underline{\boldsymbol{0}}} \\ \underline{\underline{\boldsymbol{0}}} & \underline{\underline{\boldsymbol{K}}}_{1,1}^{-1} \end{bmatrix},$$

where the inverses of the diagonal blocks are applied separately, with appropriate solvers and associated preconditioners.

$$\underline{\underline{\boldsymbol{K}}}_{0,0}^{-1} \approx \begin{bmatrix} \underline{\underline{\boldsymbol{I}}} & -\underline{\underline{\widetilde{\boldsymbol{A}}}}^{-1}\underline{\underline{\boldsymbol{B}}}^T \\ \underline{\underline{\boldsymbol{0}}} & \underline{\underline{\boldsymbol{I}}} \end{bmatrix} \begin{bmatrix} \underline{\underline{\widetilde{\boldsymbol{A}}}}^{-1} & \underline{\underline{\boldsymbol{0}}} \\ \underline{\underline{\boldsymbol{0}}} & \underline{\underline{\boldsymbol{S}}}^{-1} \end{bmatrix},$$

where $\underline{\underline{\boldsymbol{S}}} = -\underline{\underline{\boldsymbol{B}}}\,\underline{\underline{\widetilde{\boldsymbol{A}}}}^{-1}\underline{\underline{\boldsymbol{B}}}^T$.

Reduced Basis Method

Problem considered

Given $\mu \in D^\mu$, evaluate the output of interest

$$s_N(\mu) = \ell(\boldsymbol{T}^{\mathrm{rbm},N}(\mu); \mu)$$

where $\boldsymbol{T}^{\mathrm{rbm},N}(\mu) \in V_N$ is the solution of

$$a(\boldsymbol{T}^{\mathrm{rbm},N}(\mu), v; \mu) = f(v; \mu) \quad \forall v \in V_N$$

- *Snapshots matrix:* $\mathbb{Z}_N = [\xi_1, \cdots, \xi_N] \in \mathbb{R}^{\mathcal{N} \times N}$,

Reduced Basis Method

Problem considered

Given $\mu \in D^{\mu}$, evaluate the output of interest

$$s_N(\mu) = \ell(\boldsymbol{T}^{\mathrm{rbm},N}(\mu); \mu)$$

where $\boldsymbol{T}^{\mathrm{rbm},N}(\mu) \in V_N$ is the solution of

$$a(\boldsymbol{T}^{\mathrm{rbm},N}(\mu), v; \mu) = f(v; \mu) \quad \forall v \in V_N$$

- *Snapshots matrix:* $\mathbb{Z}_N = [\xi_1, \cdots, \xi_N] \in \mathbb{R}^{\mathcal{N} \times N}$,
- Projection onto V_N: $\boxed{\underline{\underline{\boldsymbol{A}}}_N(\mu) := \mathbb{Z}_N^T \underline{\underline{\boldsymbol{A}}}(\mu) \mathbb{Z}_N \in \mathbb{R}^{N \times N}}$ and $\boldsymbol{f}_N(\mu) := \mathbb{Z}_N^T \boldsymbol{f}(\mu) \in \mathbb{R}^N$,

Reduced basis resolution

Input: $\mu \in D^{\mu}$,

- Construct $\underline{\underline{\boldsymbol{A}}}_N(\mu)$, $\boldsymbol{f}_N(\mu)$ and $\boldsymbol{L}_{N,k}(\mu)$,
- Solve $\underline{\underline{\boldsymbol{A}}}_N(\mu) \boldsymbol{T}^{\mathrm{rbm},N}(\mu) = \boldsymbol{f}_N(\mu)$,
- Compute outputs $s_{N,k}(\mu) = \boldsymbol{L}_{N,k}(\mu)^T \boldsymbol{T}^{\mathrm{rbm},N}(\mu)$.

Output: Numerical solution $\boldsymbol{T}^{\mathrm{rbm},N}(\mu)$ and outputs $s_{N,k}(\mu)$.

Affine decomposition[a]

- We want to write $\underline{\underline{\boldsymbol{A}}}(\mu) = \sum_{q=1}^{Q_a} \beta_A^q(\mu)\underline{\underline{\boldsymbol{A}}}^q$, and $\boldsymbol{F}(\mu) = \sum_{q=1}^{Q_f} \beta_F^q(\mu)\boldsymbol{F}^q$.
- Compute and store $\underline{\underline{\boldsymbol{A}}}_N^q = \underbrace{\mathbb{Z}_N^T \underline{\underline{\boldsymbol{A}}}^q \mathbb{Z}_N}_{\text{independent of } \mu}$ and $\boldsymbol{F}_N^q = \mathbb{Z}_N^T \boldsymbol{F}^q$.
- Hence, $\underline{\underline{\boldsymbol{A}}}_N(\mu) = \sum_{q=1}^{Q_a} \beta_A^q(\mu)\underline{\underline{\boldsymbol{A}}}_N^q$ and $\boldsymbol{F}_N(\mu) = \sum_{q=1}^{Q_f} \beta_F^q(\mu)\boldsymbol{F}_N^q$.

[a] Prud'homme *et al.* *Journal of Fluids Engineering*. (2002)

Affine decomposition[a]

- We want to write $\underline{\underline{\boldsymbol{A}}}(\mu) = \sum_{q=1}^{Q_a} \beta_A^q(\mu) \underline{\underline{\boldsymbol{A}}}^q$, and $\boldsymbol{F}(\mu) = \sum_{q=1}^{Q_f} \beta_F^q(\mu) \boldsymbol{F}^q$.
- Compute and store $\underline{\underline{\boldsymbol{A}}}_N^q = \mathbb{Z}_N^T \underline{\underline{\boldsymbol{A}}}^q \mathbb{Z}_N$ and $\boldsymbol{F}_N^q = \mathbb{Z}_N^T \boldsymbol{F}^q$.
- $a(T, v; \mu) = \sum_{q=1}^{4} \beta_A^q(\mu) a^q(T, v)$ with

$$
\begin{aligned}
\beta_A^1(\mu) &= k_{\text{lens}} & a^1(T, v) &= \int_{\Omega_{\text{lens}}} \nabla T \cdot \nabla v \,\mathrm{d}x \\
\beta_A^2(\mu) &= h_{\text{amb}} & a^2(T, v) &= \int_{\Gamma_{\text{amb}}} T v \,\mathrm{d}\sigma \\
\beta_A^3(\mu) &= h_{\text{bl}} & a^3(T, v) &= \int_{\Gamma_{\text{body}}} T v \,\mathrm{d}\sigma \\
\beta_A^4(\mu) &= 1 & a^4(T, v) &= \int_{\Gamma_{\text{amb}}} h_r T v \,\mathrm{d}\sigma + \sum_{i \neq \text{lens}} k_i \int_{\Omega_i} \nabla T \cdot \nabla v \,\mathrm{d}x
\end{aligned}
$$

[a] Prud'homme *et al.* *Journal of Fluids Engineering.* (2002)

Affine decomposition[a]

- We want to write $\underline{\underline{\boldsymbol{A}}}(\mu) = \sum_{q=1}^{Q_a} \beta_A^q(\mu) \underline{\underline{\boldsymbol{A}}}^q$, and $\boldsymbol{F}(\mu) = \sum_{q=1}^{Q_f} \beta_F^q(\mu) \boldsymbol{F}^q$.
- Compute and store $\underline{\underline{\boldsymbol{A}}}_N^q = \mathbb{Z}_N^T \underline{\underline{\boldsymbol{A}}}^q \mathbb{Z}_N$ and $\boldsymbol{F}_N^q = \mathbb{Z}_N^T \boldsymbol{F}^q$.
- $f(v;\mu) = \sum_{p=1}^{2} \beta_F^p(\mu) f^p(v)$

$$\beta_F^1(\mu) = h_{\text{amb}} T_{\text{amb}} + h_r T_{\text{amb}} - E \qquad f^1(v) = \int_{\Gamma_{\text{amb}}} v \, \mathrm{d}\sigma$$

$$\beta_F^2(\mu) = h_{\text{bl}} T_{\text{bl}} \qquad f^2(v) = \int_{\Gamma_{\text{body}}} v \, \mathrm{d}\sigma$$

[a] Prud'homme *et al.* *Journal of Fluids Engineering*. (2002)

Offline / Online procedure

Offline:

- Solve N high-fidelity systems depending on $\mathcal{N}$ to form $\mathbb{Z}_N$,
- Form and store $\boldsymbol{F}_N^p(\xi_i)$
- Form and store $\underline{\underline{\boldsymbol{A}}}_N^q(\xi_i)$

Online: independant of $\mathcal{N}$

Given a new parameter $\mu \in D^\mu$,

- Form $\underline{\underline{\boldsymbol{A}}}_N(\mu)$: $O(Q_a N^2)$,
- Form $\boldsymbol{F}_N(\mu)$: $O(Q_f N)$,
- Solve $\underline{\underline{\boldsymbol{A}}}_N(\mu)\boldsymbol{T}^{\text{rbm},N}(\mu) = \boldsymbol{F}_N(\mu)$: $O(N^3)$,
- Compute $s_N(\mu) = \boldsymbol{L}_N(\mu)^T \boldsymbol{T}^{\text{rbm},N}(\mu)$: $O(N)$.

Error bound[a] $\Delta_N(\mu)$

Such an error bound can be constructed efficiently from the *residual* r of the variational problem:

$$r(v,\mu) := \ell(v;\mu) - a(T^{\mathrm{rbm},N}(\mu), v;\mu) \quad \forall v \in V$$

a lower bound $\alpha_{\mathrm{lb}}(\mu)$ of the coercivity constant $\alpha(\mu)$ of $a(\cdot,\cdot;\mu)$, and the affine decomposition of a and f:

$$\Delta_N^s(\mu) := \frac{\|r(\cdot,\mu)\|_{V'}^2}{\alpha_{\mathrm{lb}}(\mu)}$$

[a] Prud'homme *et al.* *Journal of Fluids Engineering*. (2002)

Greedy algorithm

Algorithm 1: Greedy algorithm to construct the reduced basis.

Input: $\mu_0 \in D^\mu$, $\Xi_{\text{train}} \subset D^\mu$ and $\varepsilon_{\text{tol}} > 0$
$S \leftarrow [\mu_0]$;
while $\Delta_N^{\max} > \varepsilon_{tol}$ **do**
$\quad \mu^\star \leftarrow \arg\max_{\mu \in \Xi_{\text{train}}} \Delta_N(\mu)$ (and $\Delta_N^{\max} \leftarrow \max_{\mu \in \Xi_{\text{train}}} \Delta_N(\mu)$);
$\quad V_{N+1} \leftarrow \left\{ \boldsymbol{\xi} = \boldsymbol{T}^{\text{fem}}(\mu^\star) \right\} \cup V_N$;
$\quad$ Append $\mu^\star$ to S;
$\quad N \leftarrow N + 1$;
end
Output: Sample S, reduced basis V_N

NIRB method[a]

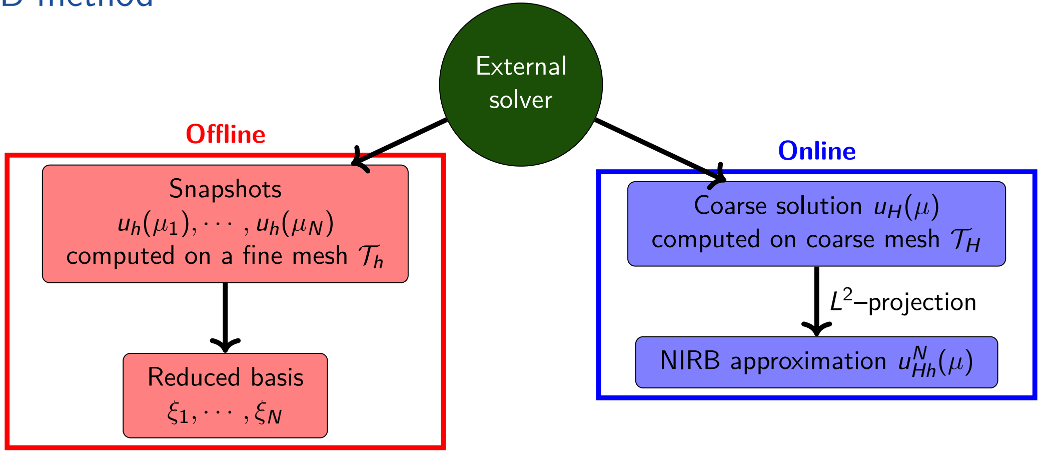

[a] Chakir & Maday *Comptes Rendus Mathématique*. (2009)

NIRB method[a]

Instead of solving the system $\underline{\underline{\boldsymbol{A}}}^N(\mu)\boldsymbol{U}_h^N(\mu) = \boldsymbol{F}^N(\mu)$ in the online stage and construct the solution by :

$$u_h^N(\mu) = \sum_{i=1}^{N} \boldsymbol{U}_{h,i}^N(\mu)\xi_i$$

Let's denote by $\Pi_N u_h$ the L^2- projection of $\mathbb{FE}$ approximation u_h in the space X_h^N :

$$\Pi_N u_h(\mu) = \sum_{i=1}^{N} \alpha_i^{N,h}(\mu)\xi_i$$

Due to the orhtonormalization of basis function ξ_i, $\alpha_i^{N,h}(\mu)$ are defined by :

$$\alpha_i^{N,h}(\mu) = \langle u_h(\mu), \xi_i \rangle_{L^2}$$

[a] Chakir & Maday *Comptes Rendus Mathématique*. (2009)

- **Coarse** triangulation : $\{\mathcal{T}_H\}_H$ with $H \gg h$,
- new finite element space : X_H such that $\mathcal{N}_H = \dim(X_H) \ll \dim(X_h) = \mathcal{N}_h$,
- the computation of $u_H(\mu) \in X_H$ is less expensive than the one of $u_h(\mu) \in X_h$

The **NIRB method** consists in proposing another alternative of $\alpha_i^{N,h}(\mu)$ defined by :

$$\alpha_i^{N,H}(\mu) = \langle u_H(\mu), \xi_i \rangle_{L^2} \,,$$

with $u_H(\mu)$, an approximate solution of the high-fidelity problem in the coarse triangulation.

Neural Networks

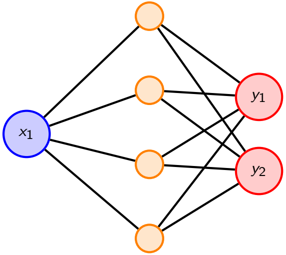

- Neural Network: $NN\colon \boldsymbol{x} \in \mathbb{R}^p \mapsto \boldsymbol{y} \in \mathbb{R}^q$
- $NN(\boldsymbol{x}) = f_p \circ \sigma \circ f_{p-1} \circ \sigma \circ \cdots \circ f_1(\boldsymbol{x})$, where:
  - f_i are affine functions $f_i(\boldsymbol{x}) = \underline{\underline{\boldsymbol{W}}}_i \boldsymbol{x} + \boldsymbol{b}_i$
  - σ is a *non-linear activation* function (*e.g.* sigmoid, ReLu...).
- $\underline{\underline{\boldsymbol{\Theta}}} = (\underline{\underline{\boldsymbol{W}}}_1, \boldsymbol{b}_1, \ldots, \underline{\underline{\boldsymbol{W}}}_p, \boldsymbol{b}_p)$.

Density of neural networks[a]

The space of neural networks functions with 1 hidden layer ($p = 1$) is dense in the space of continuous functions on a compact set, for the norm $\|\cdot\|_\infty$.

[a] Cybenko *Mathematics of Control, Signals, and Systems.* (1989)

Neural Networks: training

- Set of data: $D = \{(\boldsymbol{x}_j, \boldsymbol{y}_j)\}_{j=1}^{N}$
- Loss function: $\text{Loss}(\underline{\underline{\boldsymbol{\Theta}}}) = \sum_{(\boldsymbol{x},\boldsymbol{y})\in D} \left| NN_{\underline{\underline{\boldsymbol{\Theta}}}}(\boldsymbol{x}) - \boldsymbol{y} \right|^2$
- Optimization: look for $\underline{\underline{\boldsymbol{\Theta}}}^\star = \arg\min_{\underline{\underline{\boldsymbol{\Theta}}}} \text{Loss}(\underline{\underline{\boldsymbol{\Theta}}})$
- **Least square theorem:** The solution exists. It is unique if the data is linearly independent.

Physics-Informed Neural Networks[a]

- Combines both unsupervised and supervised learning.
- Trained to solve learning tasks while respecting a law given here by the ODE / PDE **and** provided data.
- « $\text{Loss} = \text{Loss}_{\text{model}} + \text{Loss}_{\text{data}}$ »

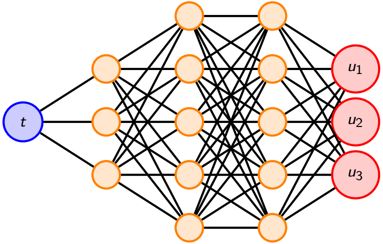

Input size = 3 size = 5 size = 5 Output

[a] Raissi *et al.* *Journal of Computational Physics*. (2019)